

AFIT/GAE/ENY/93D-2

AD-A273 729



DTIC  
ELECTE  
DEC 16 1993  
S A

THESIS

ANALYSIS OF THE EFFECTS OF WAKE PASSAGE ON  
HEAT TRANSFER IN A LINEAR TURBINE CASCADE

Kevin Scott Allen, B.S.A.E.  
Captain, USAF

AFIT/GAE/ENY/93D-2

93-30411



This document has been approved  
for public release and sale; its  
distribution is unlimited.

93 12 15081

The views expressed in this thesis are those of the author and do not reflect the official policy or position of the Department of Defense or the United States Government.

Accession For	
NTIS CRA&I	<input checked="checked" type="checkbox"/>
DTIC TAB	<input type="checkbox"/>
Unannounced	<input type="checkbox"/>
Justification	
By	
Distribution /	
Availability Codes	
Dist	Avail and/or Special
A-1	



AFIT/GAE/ENY/93D-2

**ANALYSIS OF THE EFFECTS OF WAKE PASSAGE ON HEAT TRANSFER IN  
A LINEAR TURBINE CASCADE**

**THESIS**

Presented to the Faculty of the Graduate School of  
Engineering of the Air Force Institute of Technology  
Air University

In Partial Fulfillment of the  
Requirements for the Degree of  
Master of Science in Aeronautical Engineering

Kevin Scott Allen, B.S.A.E.

Captain, USAF

December 1993

Approved for public release; distribution unlimited

### Acknowledgements

The purpose of this study was to quantify the effects of the passage of a wake on the heat transfer in a turbine cascade and infer from that how wake passage affects the heat transfer in a turbine engine. Having said that I would like to take this opportunity to thank the people that made this possible.

First and foremost I would like to thank my family. Without, my wife, Pat's understanding and patience this would have been impossible. And without, my daughter, Jennifer's constant presence to remind me that life goes on outside AFIT and that everything important is learned in Kindergarten, I might have given up.

On a more practical level I would like to thank my advisor, Dr. Paul I. King, for his guidance and my other committee members for their suggestions. A special thanks is offered to Tim Hancock from the AFIT model shop for the hours put in on this project and the patience he displayed when changes were made. More importantly, I would like to thank Lt Jim Braunschneider for the work he put forth in making the TCTF work as advertised and making the hours of data taking bearable.

Lastly, thanks to my many friends at AFIT for inspiration and humor.

- K. Scott Allen

## Table of Contents

Acknowledgements . . . . .	ii
List of Figures . . . . .	iv
List of Tables . . . . .	vi
List of Symbols . . . . .	vii
Abstract . . . . .	ix
I INTRODUCTION . . . . .	1
1.1 General . . . . .	1
1.2 Overview . . . . .	2
1.3 Method . . . . .	4
II THEORY . . . . .	5
2.1 General . . . . .	5
2.2 Cascade Theory . . . . .	5
2.3 Heat Transfer Theory . . . . .	7
3.1 General . . . . .	14
3.2 Turbine Cascade Test Facility . . . . .	14
3.3 Instrumentation and Data Acquisition Equipment . . . . .	20
3.4 Software . . . . .	27
IV RESULTS . . . . .	34
4.1 General . . . . .	34
4.2 Cascade Flow Characterization . . . . .	34
4.3 Test Plan . . . . .	53
4.4 Effects of Wake Passing . . . . .	55
V CONCLUSIONS AND RECOMMENDATIONS . . . . .	83
5.1 General . . . . .	83
5.2 Apparatus . . . . .	83
5.3 Wake Effects . . . . .	84
5.4 Future Experiments . . . . .	85
List of References . . . . .	88
APPENDIX I . . . . .	91
VITA . . . . .	93

## List of Figures

Figure 1 - Plexiglass top and pulley/belt/bar assembly. . . . .	15
Figure 2 - Drive motor and bar passing assembly. . . . .	17
Figure 3 - Top view of cascade showing blade numbering. . . . .	17
Figure 4 - Forward bar guide and assembly side view. . . . .	19
Figure 5 - Aft bar guide and assembly side view. . . . .	19
Figure 6 - Blade #2 thermocouple locations. . . . .	24
Figure 7 - Coefficient of pressure curves for $Re_{exit} = 341,100$ . . . . .	36
Figure 8 - Coefficient of pressure curves for $Re_{exit} = 454,800$ . . . . .	37
Figure 9 - Plane 1 $U_x$ 's $Re_{exit} = 341,100$ . . . . .	39
Figure 10 - Plane 2 $U_x$ 's $Re_{exit} = 341,100$ . . . . .	39
Figure 11 - Plane 3 $U_x$ 's $Re_{exit} = 341,100$ . . . . .	40
Figure 12 - Plane 4 $U_x$ 's $Re_{exit} = 341,100$ . . . . .	40
Figure 13 - Plane 5 $U_x$ 's $Re_{exit} = 341,100$ . . . . .	41
Figure 14 - Plane 1 $U_x$ 's $Re_{exit} = 454,800$ . . . . .	41
Figure 15 - Plane 2 $U_x$ 's $Re_{exit} = 454,800$ . . . . .	42
Figure 16 - Plane 3 $U_x$ 's $Re_{exit} = 454,800$ . . . . .	42
Figure 17 - Plane 4 $U_x$ 's $Re_{exit} = 454,800$ . . . . .	43
Figure 18 - Plane 5 $U_x$ 's $Re_{exit} = 454,800$ . . . . .	43
Figure 19 - Plane 1 angles $Re_{exit} = 341,100$ . . . . .	44
Figure 20 - Plane 2 angles $Re_{exit} = 341,100$ . . . . .	44
Figure 21 - Plane 3 angles $Re_{exit} = 341,100$ . . . . .	45
Figure 22 - Plane 4 angles $Re_{exit} = 341,100$ . . . . .	45
Figure 23 - Plane 5 angles $Re_{exit} = 341,100$ . . . . .	46
Figure 24 - Plane 1 angles $Re_{exit} = 454,800$ . . . . .	46
Figure 25 - Plane 2 angles $Re_{exit} = 454,800$ . . . . .	47
Figure 26 - Plane 3 angles $Re_{exit} = 454,800$ . . . . .	47
Figure 27 - Plane 4 angles $Re_{exit} = 454,800$ . . . . .	48
Figure 28 - Plane 5 angles $Re_{exit} = 454,800$ . . . . .	48
Figure 29 - Local chord based Reynolds number over the surface of the blade, $Re_{exit} = 341,100$ . . . . .	50
Figure 30 - Topographical Plot of total pressure loss coefficient, plane 2, $Re_{exit} = 341,100$ . . . . .	52
Figure 31 - Convective heat transfer coefficient (h) over the surface of the blade, $Re_{exit} = 341,100$ . . . . .	61
Figure 32 - Convective heat transfer coefficient (h) over the surface of the blade, $Re_{exit} = 454,800$ . . . . .	62
Figure 33 - Local Nusselt number over the surface of the blade, $Re_{exit} = 341,100$ . . . . .	65
Figure 34 - Local Nusselt number over the surface of the blade, $Re_{exit} = 454,800$ . . . . .	66
Figure 35 - Local Stanton number over the surface of the blade, $Re_{exit} = 341,100$ . . . . .	68
Figure 36 - Local Stanton number over the surface of the blade, $Re_{exit} = 454,800$ . . . . .	69

Figure 37 - Local Frössling number over the surface of the blade, $Re_{exit} = 341,100$ . . . . .	72
Figure 38 - Local Frössling number over the surface of the blade, $Re_{exit} = 454,800$ . . . . .	73
Figure 39 - Stagnation Frössling number, $Nu$ based on chord length, $Re$ based on freestream velocity and chord length, versus bar passing Strouhal number. . . . .	74
Figure 40 - Stagnation $Nu_c$ over bar out $Nu_c$ versus bar passing Strouhal number. . . . .	74
Figure 41 - Nusselt numbers compared with Meschwitz's (1991) 10% turbulence data, $Re_{exit} = 454,800$ . . . . .	76
Figure 42 - Comparison of analytical data and empirical solns. of $Nu_i$ versus $Re_i$ , suction surface, $Re_{exit} = 341,100$ . . . . .	80
Figure 43 - Comparison of analytical data and empirical solns. of $Nu_i$ versus $Re_i$ , pressure surface, $Re_{exit} = 341,100$ . . . . .	80
Figure 44 - Comparison of analytical data and empirical solns. for $Nu_i$ versus $Re_i$ , suction surface, $Re_{exit} = 454,800$ . . . . .	81
Figure 45 - Comparison of analytical data and empirical solns. of $Nu_i$ versus $Re_i$ , pressure surface, $Re_{exit} = 454,800$ . . . . .	81
Figure 46 - Raw temperature data for the 23 exterior thermocouples, $Re_{exit} = 341,100$ . . . . .	91
Figure 47 - Raw temperature data for the 23 exterior thermocouples, $Re_{exit} = 454,800$ . . . . .	92

### List of Tables

Table 1 - Thermocouple and Pressure Tap Locations . . .	25
Table 2 - Scanivalve Port Assignments . . . . .	30
Table 3 - Test Plan . . . . .	54



## List of Symbols

Symbol:	Definition:
$c$	True normal chord length, 0.1143 m (4.5 in.)
$c_{air}$	Specific heat of air (J/(kg K))
$C_p$	Coefficient of pressure
$d$	Length parameter (m)
$d_b$	Diameter of wake generating bars, 1.988 mm (0.07825 in.)
$f_b$	Bar passing frequency (Hz)
$h$	Convective heat transfer coefficient (W/(m <sup>2</sup> K))
$I_{foil}$	Current in the heat transfer foil (amps)
$k_{air}$	Thermal conductivity of air (W/(m K))
$k_{blade}$	Thermal conductivity of urethane foam (W/(m K))
$Nu_c$	Nusselt number based on chord length
$Nu_l$	Local Nusselt number based on surface location
$P_0$	Total pressure (Pa)
$P_l$	Local static pressure (Pa)
$Pr$	Prandtl Number
$P_{static}$	Static pressure (Pa)
$P_\infty$	Freestream static pressure, behind bars (Pa)
$q_{cond}''$	Conductive heat flux (W/m <sup>2</sup> )
$q_{conv}''$	Convective heat flux (W/m <sup>2</sup> )
$q_{rad}''$	Radiative heat flux (W/m <sup>2</sup> )
$q_{tot}''$	Total heat flux (W/m <sup>2</sup> )
$R$	Gas constant (J/(kg K))
$Re_{exit}$	Reynolds number at the cascade exit
$Re_l$	Local Reynolds number, on the blade's surface
$Re_{lc}$	Local Reynolds number, based on chord length
$Re_\infty$	Freestream Reynolds number
$R_{foil}$	Resistance of the heat transfer foil per unit area (ohms/m <sup>2</sup> )
$s$	Surface length (m)
$S_b$	Bar passing Strouhal number
$S_{cascade}$	Cascade wake passing time scale
$S_{engine}$	Representative turbine engine wake passing time scale
$St$	Stanton number
$St_l$	Laminar Stanton number, from empirical equation
$St_t$	Turbulent Stanton number, from empirical equation
$t$	Unit time (s)
$T$	Temperature (K)
$T_f$	Film temperature (K)
$t_{flow}$	Time for fluid particle to traverse the length of the blade (s)
$T_{gas}$	Gas temperature (K)
$T_l$	Local surface temperature (K)
$t_w$	Time between wake passings (s)

$T_{wall}$	Wall or blade surface temperature (K)
$T_{\infty}$	Freestream temperature (K)
$u_{ave}$	Average velocity between freestream and exit (m/s)
$u_{exit}$	Exit velocity (m/s)
$u_l$	Local surface velocity (m/s)
$u_x$	Velocity in 'x' or through engine direction (m/s)
$u_{\infty}$	Freestream velocity (m/s)
$w$	Heat transfer foil width, 50.8 mm (2 in.)
$x$	Length along chord (m)

Greek symbols:

$\alpha$	Thermal diffusivity ( $m^2/s$ )
$\alpha_{air}$	Thermal diffusivity of air ( $m^2/s$ )
$\epsilon$	Emissivity of heat transfer foil
$\mu$	Dynamic viscosity of air ( $kg/(m \ s)$ )
$\rho_{air}$	Density of air ( $kg/m^3$ )
$\rho_{fluid}$	Density of manometer indicating fluid ( $kg/m^3$ )
$\rho_{foil}$	Resistivity of heat transfer foil ( $\Omega \ m$ )
$\rho_{H2O}$	Density of water ( $kg/m^3$ )
$\rho_l$	Local density ( $kg/m^3$ )
$\rho_{\infty}$	Freestream density ( $kg/m^3$ )
$\sigma$	Stefan-Boltzman constant ( $W/(m^2K^4)$ )
$\nu$	Kinematic viscosity ( $m^2/s$ )

Abstract

This study investigated the effect of wake passage on the heat transfer in a linear turbine cascade. The apparatus used was the Air Force Institute of Technology linear Turbine Cascade Test Facility (TCTF). The TCTF was fitted with a belt and pulley system to facilitate a series of translating bars. The bars, when passed upstream of the cascade, created a series of wakes. The parameters varied were freestream model Reynolds number and bar conditions, i.e., bars in, bars out, and bar passing frequency. One blade in the TCTF was instrumented to allow pressure and temperature measurements at discrete points on the blade's surface. From the pressure and temperature data the convective heat transfer coefficient at these discrete locations was calculated. Results were compared to previous TCTF heat transfer data, empirical solutions, and other wake passage experiments. For all tests with closely spaced bars, the effect of wake passing on the heat transfer of the blade was similar to the effect of grid-generated 10% freestream turbulence on the cascade.

## I INTRODUCTION

### 1.1 General

The objective of this research was to determine the effect of wake passage on the mean convective heat transfer of a blade surface in a linear turbine cascade. Variations in model Reynolds number and wake passage frequency and their effects were also studied.

The experiments were performed in the Air Force Institute of Technology (AFIT) linear Turbine Cascade Test Facility (TCTF). The method of using a linear turbine cascade as a testbed has been validated throughout many years of experimentation (Oates, 1985). In addition, AFIT's linear turbine cascade is modeled after a previous design and the performance of both cascades has been validated and quantified in numerous experiments, including Gallasi (1989), Acree (1990) and Meschwitz (1991). The TCTF and the associated hardware are described in detail in Chapter III.

Previous experimental efforts on the TCTF and other experimental setups have found that turbine blade heat transfer is a function of many parameters. Included in these parameters are the model Reynolds number, cascade geometry, blade geometry, freestream turbulence intensity and wake passage (Doorly, 1984). Research efforts by Gallasi (1989), Acree (1990), and Meschwitz (1991) investigated all of the above parameters excepting wake

passage. Doorly investigated the effects of wake passage on turbine blade heat transfer. However, Doorly's experimental apparatus used a high speed wind tunnel with rotating bars fixed to a disk that was mounted forward of a cascade of turbine blades. In Doorly's experiment, and those of many others using a similar apparatus, e.g. O'Brien (1988), Hilditch and Ainsworth (1990), Schultz and LeGraff (1987), Ainsworth and LeGraff (1989), and Dullenkopf, Schultz, and Wittig (1990), attempts were made to match some turbine engine operating conditions. Specifically, the time scales (discussed in Chapter II), which measure the ratio of the time between wakes to pass a point in space and the time for a fluid particle to traverse the length of the passage, were closely matched to those of an engine. Somewhat smaller time scales were used in this experiment than in those mentioned above. On the other hand, some three dimensional effects inherent in an axisymmetric wind tunnel, such as Doorly's apparatus, were avoided in this experiment. However, the results of the experiment of Doorly, and others using the rotating bar apparatus, were valuable in analyzing the results of this experiment.

## 1.2 Overview

Each of the aforementioned experiments has built onto the body of knowledge about turbine blade heat transfer.

Works by Doorly (1984) and Dullenkopf, et al. (1990) have attempted to look into the turbine blade's boundary layer, and its associated heat transfer, and examine how it was affected by wake passage. Still others, Tran, et al. (1991), Rigby, et al. (1989), Johnson, et al. (1989), have taken Doorly's, and others', data and tried to model it in one way or another, with varying degrees of success. However, questions still exist about how to model the effects of wake passage on turbine blade heat transfer. By comparison of the results of this experiment and those of others (Meschwitz, Doorly, Dullenkopf, etc.), the present study has attempted to answer some of these lingering questions.

More important though was the metamorphosis of the TCTF into a device that can be used for studying the effects of wake passage in the future. This has given AFIT the ability to build further onto the body of knowledge of wake interaction in turbine blade heat transfer. This is an ability it did not possess previously.

The primary change to the TCTF from the experiments of previous users was the removal of the turbulence generation grid and the addition of a series of translating bars forward of the row of cascade blades. The introduction of translating bars to the flow forward of the blade row created a series of wakes behind the bars that impinged on

the blades. By instrumenting one of the blades to determine heat transfer from the blade to the flow, and learning the character of the flow around the instrumented blade, conclusions were drawn as to the effects of wake passage.

### 1.3 Method

The majority of the hardware and nearly all of the software necessary to conduct the experiment was available in the TCTF through the efforts of Galassi (1989), Acree (1990), and Meschwitz (1991). However, significant modifications to the linear turbine cascade, structural and otherwise, were necessary to implement the translating bars.

Due to these modifications the character of the flow in the test section of the TCTF differed from that of previous experiments. Therefore, the first task was to recharacterize the flow in the cascade without wake passage effects. Secondly, a characterization of the flow including wakes was accomplished. Once this was complete, a test plan was formulated which allowed for variations in model Reynolds number and wake passage frequency. The data from the various runs was then analyzed, conclusions drawn, and comparisons made to other efforts where possible.

## II THEORY

### 2.1 General

This chapter reviews the theories associated with cascade flow and heat transfer. The primary concern was in the area of heat transfer. As a result, most of the theory is dedicated to that end. The discussion of cascade theory is limited to the characterization of the cascade flow. For a more extensive discussion of cascade theory see Dixon (1989).

### 2.2 Cascade Theory

Certain flow properties are necessary in the cascade for it to be considered "well-behaved" and allow the results of one study to be considered against another.

#### 2.2.1 Pressure Coefficient

The first element of cascade theory required is the non-dimensional blade pressure coefficient,  $C_p$ , defined:

$$C_p = \frac{P_l - P_\infty}{\frac{1}{2} \rho_\infty U_\infty^2} \quad (1)$$

The freestream reference in this case was the tunnel conditions upstream of the test section, but downstream of the bars (if installed).

The pressure coefficient distribution on the cascade blade surface is a good indication of cascade behavior. As



certain cascade conditions are changed, e.g., incidence angle and turbulence level (Meschwitz, 1991), the  $C_p$  distribution will change. These changes can be observed and analyzed to characterize the cascade flow.

### 2.2.2 Local Blade Isentropic Velocity

The coefficient of pressure can be manipulated to yield the local blade velocity. For steady, frictionless, incompressible flow (an assumption in this case because total pressure cannot be conserved through the cascade) along a streamline, Bernoulli's equation states:

$$p_l + \frac{1}{2}\rho_l U_l^2 = p_\infty + \frac{1}{2}\rho_\infty U_\infty^2 \quad (2)$$

The perfect gas equation of state,  $P = \rho RT$ , is used to determine the densities. By combining equations (1) and (2), the resulting expression yields:

$$U_l = \left[ \frac{2 q_\infty}{\rho_l} (1 - C_p) \right]^{\frac{1}{2}} \quad (3)$$

The temperature used in the perfect gas equation to find the local density is the film temperature,  $T_f$ , defined by:

$$T_f = \frac{T_l + T_\infty}{2} \quad (4)$$

For the purpose of this experiment, the upstream recovery temperature is taken to be  $T_\infty$ . The importance of the local velocity is seen primarily in the local Reynolds number.

### 2.2.3 Reynolds Number

The final parameter used in characterizing the cascade flow and heat transfer for this experiment is Reynolds number.  $Re$  is a non-dimensional combination of velocity, density, a length parameter,  $x$ , which can be either a blade surface length or chord length for instance, and the viscosity,  $\mu$ . This experiment will make use of four different formulations for Reynolds number, given below:

$$\begin{aligned} Re_l &= \frac{\rho_l U_l s}{\mu} \\ Re_c &= \frac{\rho_l U_l c}{\mu} \\ Re_\infty &= \frac{\rho_\infty U_\infty c}{\mu} \\ Re_{exit} &= \frac{\rho_\infty U_{exit} c}{\mu} \end{aligned} \tag{5}$$

### 2.3 Heat Transfer Theory

All three methods of heat transfer, conduction, convection, and radiation, are at work in the TCTF, and an understanding of each is required to determine the parameter of interest, the convective heat transfer coefficient ( $h$ ). In an actual turbine engine heat energy from the flow is convected and radiated to the turbine blade surface and then conducted away from the surface to the interior of the blade. In the TCTF the surface of the blade is heated with

a known energy input, and measurements are taken to determine the heat energy taken from the blade surface via conduction, convection and radiation.

The gas to wall temperature ratio ( $T_{gas}/T_{wall}$ ) is an important parameter in the amount of heat flux a turbine blade experiences. In common gas turbine engines the ratio is near 1.5 (Doorly, 1984) and can be 2 or more. For this experiment the ratio is taken below unity, an average value over the surface of the blade is near 0.95 on average, such that the blade convects heat energy to the flow rather than the flow to the blade as in an engine.

The general steady state equation for the balance of heat rate input to a point per unit area and heat rate out per unit area is:

$$q_{tot}'' = q_{cond}'' + q_{conv}'' + q_{rad}'' \quad (6)$$

#### 2.3.1 Total Heat Flux

The surface of the instrumented blade in the TCTF is electrically heated with a known energy input to a thin stainless steel foil. Given the resistance of the foil per unit surface area ( $R_{foil}$ ) and a measured current ( $I_{foil}$ ) the heat energy input to the blade surface is given by:

$$q_{tot}'' = I_{foil}^2 \cdot R_{foil} \quad (7)$$

The resistance of the foil was found to be a function of temperature by Acree (1990):

$$R_{foil} = \frac{\rho_{foil}}{w^2 t}$$

$$\rho_{foil} = 2.223 \times 10^{-10} \left( \frac{\Omega \cdot m}{^\circ F} \right) \cdot T(^{\circ}F) + 8.446 \times 10^{-7} (\Omega \cdot m)$$

While the value for  $R_{foil}$  assumes a constant width of foil transmitting the current, this is not always the case. At the points on the foil where it is attached to the power supply copper bus bars near the trailing edge on the suction and pressure surfaces, there are regions of unknown "current density" (Meschwitz, 1991). In other words the current flows through a smaller width of foil than at the other points on the blade causing radical rises in temperature at these locations. This is discussed further in Chapter III.

### 2.3.2 Radiative Heat Flux

Calculation of the radiative heat flux is based on the law of thermal radiation from Stefan-Boltzmann (Modest, 1993). The emissivity,  $\epsilon$ , is 0.17 (Meschwitz, 1991) for polished stainless steel at 300 Kelvin and the Stefan-Boltzman constant,  $\sigma$ , is  $5.67 \times 10^{-8}$  (W/(m<sup>2</sup>K<sup>4</sup>)) (Modest, 1993).

$$q_{rad}'' = \epsilon \sigma (T_i^4 - T_{\infty}^4) \quad (9)$$

### 2.3.3 Conduction Heat Flux

The conductive heat flux to the blade's core is calculated using:

$$q_{cond}'' = -k_{blade} \frac{\partial T}{\partial d} \quad (10)$$

The thermal conductivity,  $k_{blade}$ , used is the value for the instrumented blade in the TCTF, number 2. The blade is constructed of urethane foam and  $k_{blade}$  is estimated at 0.263 (W/(m K)) (Meschwitz, 1991). The value for  $\partial T/\partial d$  is taken as positive in the direction of increasing temperature, thus the negative sign in the equation.  $\partial T/\partial d$  is found using thermocouples around the surface of the blade and inside the blade along the centerline. Further discussion of the method of determining the temperature gradient can be found in the works of Gallasi (1989), Acree (1990), and Meschwitz (1991).

#### 2.3.4 Convective Heat Transfer

Convection is the most important of these methods of heat transfer. The vast majority of the blade's heat is lost through convection. The total heat flux due to convection is found from:

$$q_{conv}'' = h(T_l - T_\infty) \quad (11)$$

The value of  $h$  is the experimentally determined convective heat transfer coefficient. It is important to note that the thermocouples used had a large bead size, hindering their response time. As a result, the acquisition of discrete

data was not possible and the data presented is thus time averaged or mean heat transfer.

By substituting equations (7), and (9) through (11) into equation (6), the result is the instrumented blade's heat transfer equation:

$$I_{foil}^2 \cdot R = -k_{blade} \frac{\partial T}{\partial d} + h(T_i - T_{\infty}) + \epsilon_{foil} \sigma (T_i^4 - T_{\infty}^4) \quad (12)$$

Solving for  $h$ :

$$h = \frac{I_{foil}^2 \cdot R_{foil} + k_{blade} \frac{\partial T}{\partial d} - \epsilon_{foil} \sigma (T_i^4 - T_{\infty}^4)}{T_i - T_{\infty}} \quad (13)$$

Using the solution for  $h$ , some non-dimensional heat transfer parameters can be found. The first of these is the local Nusselt number:

$$Nu_l = \frac{h s}{k} \quad (14)$$

The variable  $s$  is the local blade surface distance from the leading edge,  $x/c = 0.0$ . Like  $Re$ ,  $Nu$  can have local and chord based ( $Nu_c$ ) values.

The second non-dimensional parameter is the Stanton number:

$$St = \frac{Nu}{Re Pr} \quad (15)$$

$Pr$  is the Prandtl number. The Prandtl number is a non-dimensional parameter equivalent to the kinematic viscosity ( $\nu$ ) divided by the thermal diffusivity ( $\alpha$ ) of air. Both are

evaluated at the film temperature. At normal room temperature Prandtl number is taken to be 0.707. The thermal diffusivity is defined by:

$$\alpha_{air} = \frac{k_{air}}{\rho_{air} c_{air}} \quad (16)$$

There are several methods by which both the Nusselt and Stanton numbers may be empirically calculated. Among these are flat plate and arbitrary surface laminar and turbulent solutions. Only the arbitrary shape empirical solutions were used by way of comparison with the analytical solutions from the TCTF's experimental runs to validate their outcome. They are:

$$St_l = 0.418 \frac{\mu^{0.5} (u_{\infty} \rho_{\infty})^{0.435}}{\left[ \int_0^x (u_{\infty} \rho_{\infty})^{1.87} dx \right]^{0.5}} \quad (17)$$

$$St_l = 0.0287 Pr^{-0.4} \frac{(T_l - T_{\infty})^{0.25} \mu^{0.2}}{\left[ \int_0^x (T_l - T_{\infty})^{1.25} (u_{\infty} \rho_{\infty}) dx \right]^{0.2}} \quad (18)$$

These equations are developed from Kays and Crawford (1993) equations (10-53) and (13-36) respectively. Nusselt number is calculated from the value for Stanton number using equation (15).

Another non-dimensional parameter useful in quantifying the data is the bar passing Strouhal number ( $S_b$ ) (O'Brien,

1988) :

$$S_b = \frac{2\pi f_b d_b}{U_\infty} \quad (19)$$

The bar diameter used is the diameter of the upstream wake generating bars, 0.07825 inches. O'Brien (1988) found that the heat transfer in the stagnation region of a cylinder in crossflow was a function of the bar passing Strouhal number.

A final non-dimensional parameter in quantifying wake passage effects is the wake passing time scale,  $S$ . The wake passing time scale is defined as the ratio of the amount of time between the wake passing a point in space to the time it takes a fluid particle to traverse the passage between the blades,  $t_{flow}/t_w$ . This is a type of nondimensional frequency:

$$S = \left[ \frac{t_{flow}}{t_w} \right] = f_b \cdot \frac{C}{U_{ave}} \quad (20)$$
$$U_{ave} = \frac{U_\infty + U_{exit}}{2}$$



### III METHODOLOGY

#### 3.1 General

In general, the data gathering equipment used in this experiment remained unchanged from the experiments of Gallasi (1989), Acree (1990), and Meschwitz (1991). However, many modifications were made to the physical structure of the TCTF, thus rendering the area immediately around the test section somewhat different from the setup known to previous experimenters. The reconfigured TCTF allowed investigating the model Reynolds number and wake passage effects on the heat transfer of its blades.

#### 3.2 Turbine Cascade Test Facility

Installing a series of translating bars to serve as wake generators required many structural modifications to the TCTF. Only those modifications affecting the test section and its performance will be discussed.

A new test section Plexiglass cover was constructed with a triangular region cut out and milled from its center to serve as the track for the bars (see Figure 1). The center triangular section and the remainder of the Plexiglass top were attached with three C-brackets that allowed the belt containing the bars to pass through. The sidewalls, shown in Figures 2 and 3, used to guide the

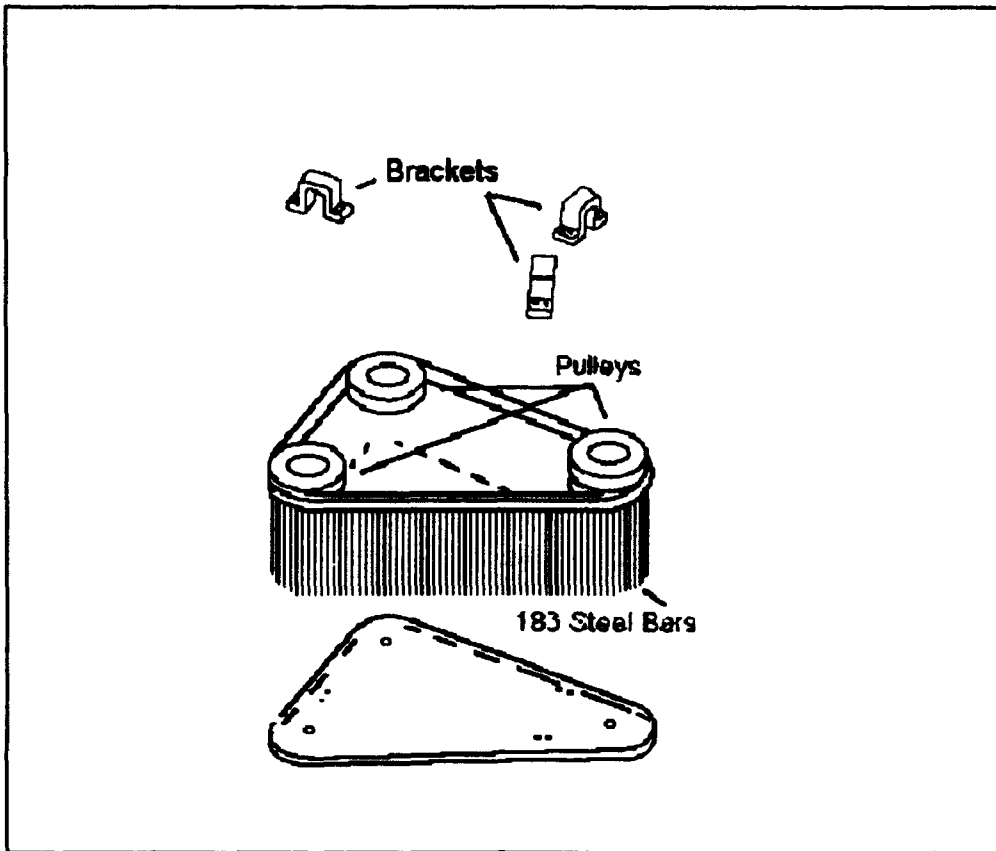


**Figure 1** - Plexiglass top and pulley/belt/bar assembly.

flow into and out of the cascade, were also modified to allow the bars to pass through. The upstream and the left (looking at Figure 3) downstream sidewalls were cut to allow the bars to pass.

The bars were  $5/64$  inch diameter drill rods cut in  $6 \pm (1/16)$  inch lengths. A total of 183 rods were installed into a 47.6 inch outer circumference double sided, automotive type V-belt, DAYCO model BB-48. The bars are spaced  $0.253 \pm 0.005$  inch apart on center and the depth of the bars in the belt was adjusted to gain  $1/16$  inch clearance from the tunnel floor. The belt was installed on the center triangular section of the plexiglass top with three pulleys as seen in Figure 1. The furthest right (looking at Figures 1 and 2) was a double pulley. The top pulley of the double pulley was driven with another V-belt attached to a variable speed drive motor, a Power Matched/R.P.M. DC Motor (see Figure 2). The motor was controlled by a variable motor controller, assembly model number DC1-70V, from Reliance Electric. By this means, the translation speed of the bars was varied and thereby also the frequency of bar passing through the cascade test section.

The diameter of the bars was chosen to produce a wake that would roughly match the size of a wake coming off the trailing edge of a stator blade of proportional size to the turbine cascade blade. This was an attempt to model what

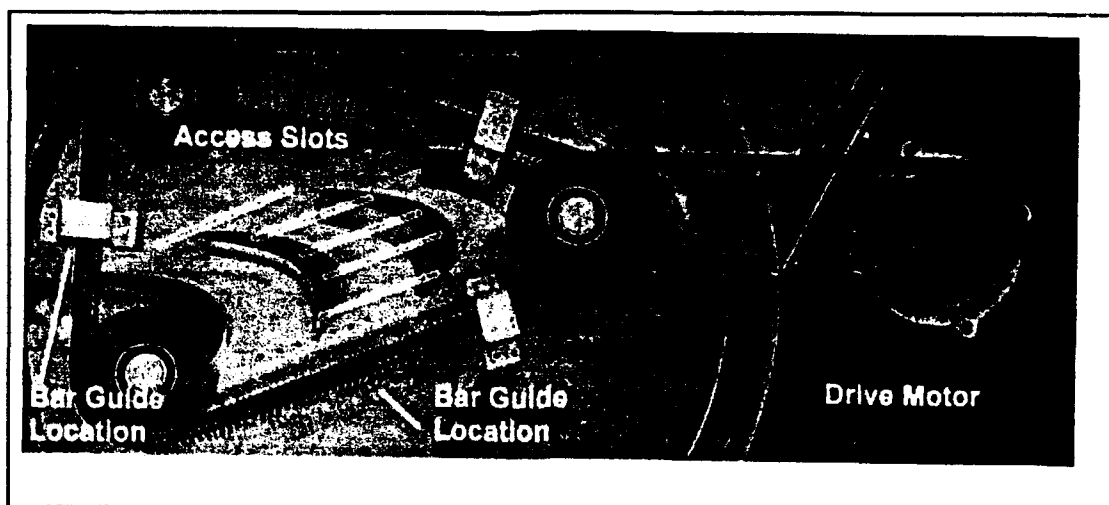


**Figure 2** - Drive motor and bar passing assembly.

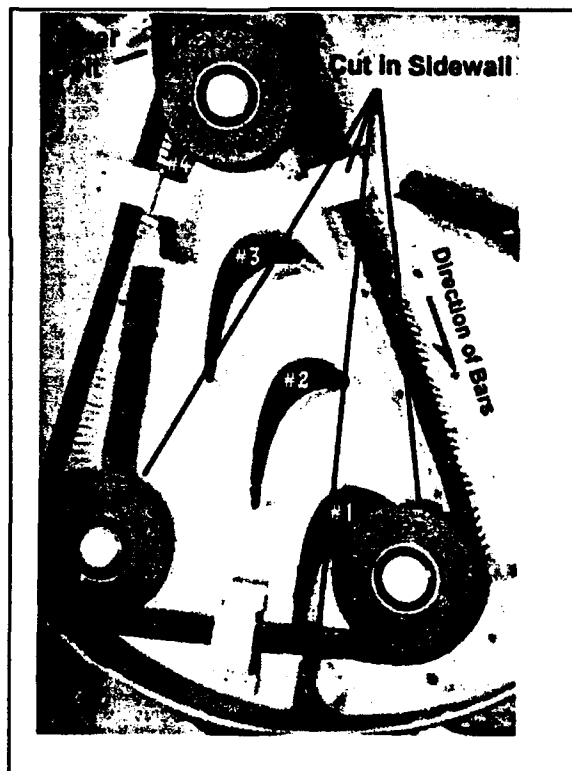


**Figure 3** - Top view of cascade showing blade numbering.

would be seen in an actual turbine engine. Also chosen to model an actual turbine was the axial spacing of the bars to the blades. The spacing was 2.25 inches, one-half of the true normal chord length.

Upon running the cascade with the bars in place, it was discovered that the bars tended to torque the belt due to the aerodynamic drag force exerted on them. The belt being of conventional rubber and nylon chord design did not have the stiffness to withstand this torque and thus allowed the bars to cant toward the test section in the front and away in the back. To prevent this from occurring guides were installed at the front and rear of the cascade passage. The forward guide was made to fit in an existing cutout in the base of the cascade. It was a height of  $1/8$  inch at its peak and tapered off at both sides to minimize flow distortion. A centered  $1/8$  inch wide groove served as the track for the bottoms of the bars (see Figure 4). It was later discovered that  $1/8$  inch of depth was not sufficient to retain the bars and an additional  $1/16$  inch of material was added to the aft side of the guide and faired into the bottom of the cascade using molding clay and speedtape. At the exit of the cascade section a single block of  $1/4$  inch thick plexiglass was installed in the base of the cascade (Figure 5) to keep the bars from swaying aft and catching the sidewalls. The effect of the installation of these

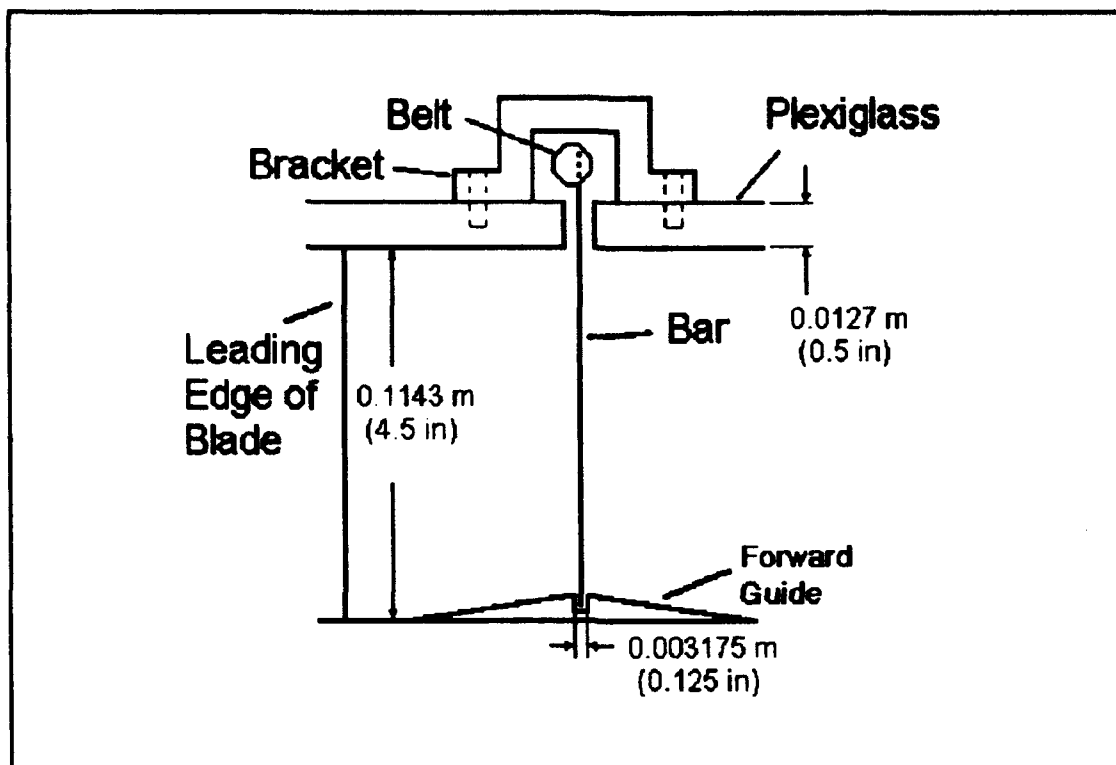


**Figure 4 - Forward bar guide and assembly side view.**

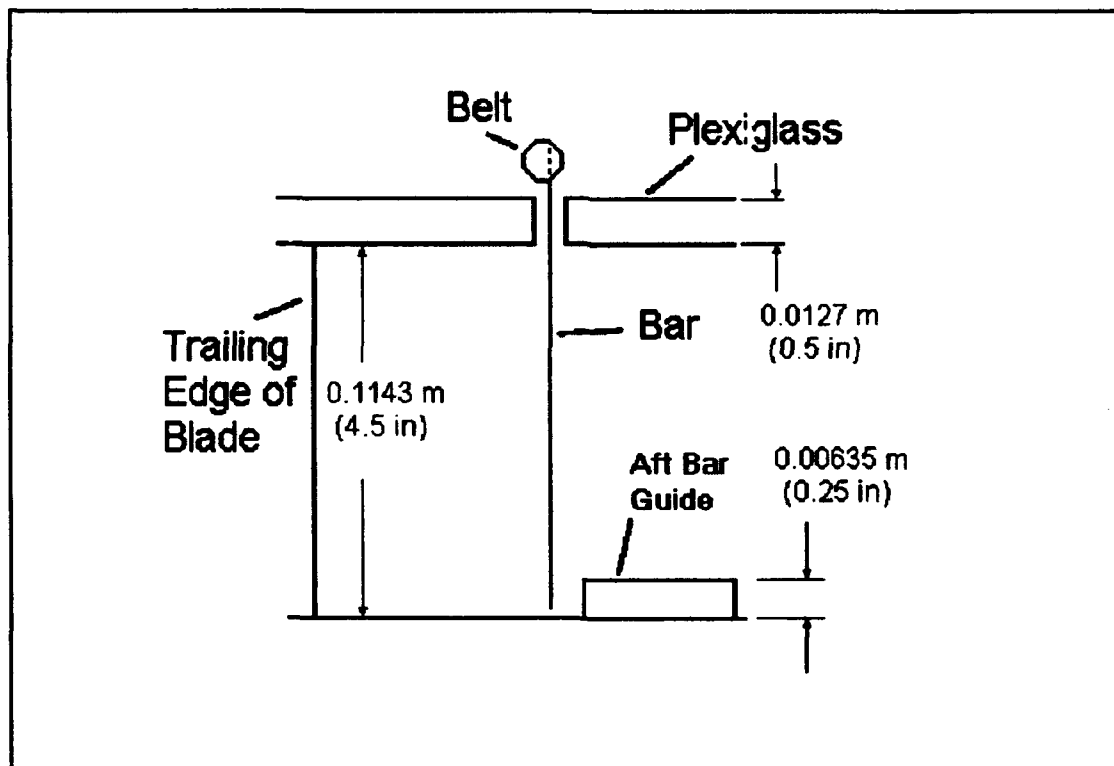


**Figure 5 - Aft bar guide and assembly side view.**

devices is discussed in Chapter IV.

Access to the cascade passage was made possible by milling five 1/4 inch slots in the triangular section of the plexiglass cover as shown in Figure 2. The slots were parallel to the leading and trailing edges of the cascade blades and spaced approximately 1 inch apart at  $x/c = 0$ , 0.26, 0.52, 0.78, and 1.05. These five slots allowed for measurements in five planes through the cascade passage, directly beneath the access slots.

Other than these modifications, made to the area around the test section, and the removal of the 16 inch long stilling chamber housing the variable geometry inlet sideboards, the TCTF hardware remained the same as that used and described by Meschwitz (1991).

### 3.3 Instrumentation and Data Acquisition Equipment

The instrumentation requirements for this experiment were largely unchanged from those of its predecessors. The exception was an additional requirement to determine the bar passing frequency. The other instrumentation requirements were for power, temperature, pressure, and velocity.

The measurement of current and voltage in the heat transfer foil on the cascade's number two blade was the lone power measurement required. Temperature measurements were required for the room air temperature (1), tunnel flow

recovery temperature (1), blade exterior heated foil temperature (23), and blade interior temperature (5). Pressure measurements were required for the blade static ports (23), upstream total pressure (1), upstream static pressure (1), and atmospheric pressure (1). Finally, velocity measurements were needed for the upstream flow and at various locations in the cascade passage.

### 3.3.1 Bar Passing Frequency Measurements

An ISSC-1262 motion detector, from Industrial Solid State Controls, employing a sensor that emits magnetic lines of flux that when broken cause the ISSC-1262 to send a pulse signal to a frequency counter-timer, RACAL-DANA model 1992, was used to determine the bar passing frequency. The bars were too closely spaced for directly measuring bar passing frequency. Instead, the frequency of the passing of a bolt attached to the drive motor pulley was found and the bar passing frequency was calculated using a function of belt distance traveled in a single revolution and the number of bars per inch:

$$f_b = f_p \cdot (11.25) \frac{\text{inches of belt}}{\text{pulley rotation}} \cdot \left( \frac{183}{47.6} \right) \frac{\text{num. of bars}}{\text{belt circum.}} \quad (21)$$

The calculated frequency was then manually recorded and input to the computer for permanent storage.



### 3.3.2 Power Measurements

As mentioned before, the number 2 (Figure 3) blade in the TCTF is the centerpiece of the cascade. A 0.002 inch thick 2 inch wide strip of stainless steel is bonded to its surface. Current is passed through the foil and through resistance it is heated. To quantify the amount of heat energy input to the foil, a measure of the current through the foil is required. The power to the foil is supplied from a Hewlet Packard HP6456B direct current power supply set to 2.5 volts d.c. and approximately 20 amps. To achieve a steady 20 amp source, a variable resistor was installed in the back of the HP6456B that served as an adjustment mechanism and would keep the current steady at 18 to 20 amps. Measurements of the current from the power supply to the foil were taken from a Weston Electric model 430 DC ammeter. The reading for amperage was manually read into the computer for use in power calculations. A Hewlet Packard HP3438A digital multimeter was used to measure the voltage across the foil, though this was primarily for the detection of any major problems with the heating foil and thermocouples.

### 3.3.3 Temperature Measurements

Blade number 2 was equipped with 23 J-type thermocouples were adhered with epoxy directly to the inside surface the heated foil, and 5 J-type thermocouples in the

blade's core along the centerline, Figure 6 and Table 1. For tunnel recovery temperature a single J-type thermocouple was placed in the boundary layer of the freestream flow upstream of the translating bars near the right sideboard. Lastly, a single J-type thermocouple was installed in an unused hot wire calibration tank that sat alongside the TCTF, for room temperature measurements. All of the thermocouples were attached to a Hewlet Packard HP2852A Data Acquisition and Control Unit using two 24 channel multiplexors and read with its integrating voltmeter. The HP2852A converted the voltages automatically to temperature in degrees Celsius and transferred the temperature to a Zenith 386 PC for storage. Room temperature could be checked with a number of thermometers in the TCTF and typically varied  $\pm 0.5$  degrees Celsius. The computer was also used to remotely program the HP2852A through an interface bus.

As mentioned in Chapter II, there were regions of unknown current density on the heat transfer foil. The current density was a result of the current channeling itself through a small area of the total foil area around the copper bus bars that supply the foil power. This, in turn, raises the foil temperature at these locations and results in erroneous heat transfer readings. For this reason points 9, 10, and 12 are deleted from the heat

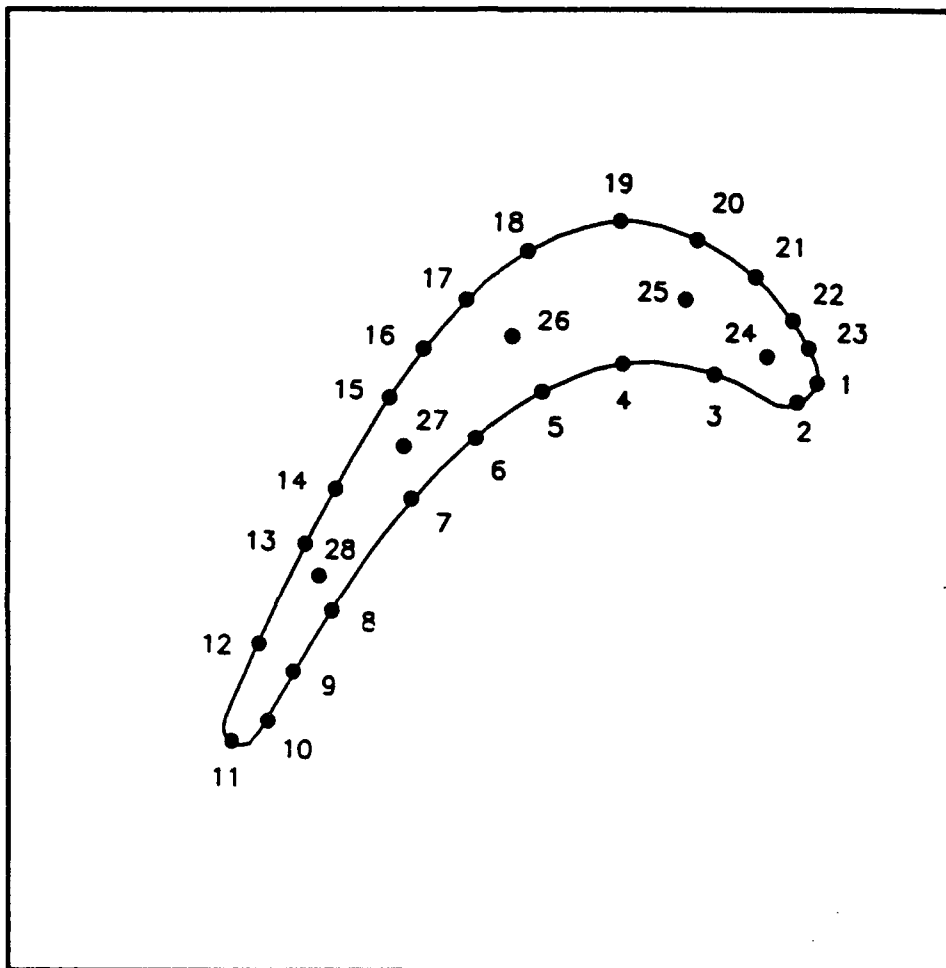


**Figure 6 - Blade #2 thermocouple locations.**

Table 1 - Thermocouple and Pressure Tap Locations

Tap #	$x/c$	$s(m)$	$s/c$	Surface
1	0.0174	0.0100	0.0875	suction
2	0.0652	0.0010	-0.0087	leading edge
3	0.1243	0.0137	-0.1199	pressure
4	0.1913	0.0280	-0.2450	pressure
5	0.3157	0.0420	-0.3675	pressure
6	0.4365	0.0615	-0.5381	pressure
7	0.6000	0.0825	-0.7218	pressure
8	0.7687	0.0930	-0.8136	pressure
9	0.8522	0.1023	-0.8950	pressure
10	0.9235	0.1085	-0.9493	pressure
11	0.9913	0.1257	1.0997	trailing edge
12	0.09026	0.1363	1.1925	suction
13	0.7643	0.1240	1.0849	suction
14	0.6670	0.1120	0.9799	suction
15	0.5817	0.1005	0.8793	suction
16	0.4870	0.0885	0.7743	suction
17	0.3852	0.0820	0.7174	suction
18	0.3322	0.0683	0.5976	suction
19	0.2191	0.0545	0.4768	suction
20	0.1078	0.0402	0.3517	suction
21	0.0357	0.0238	0.2082	suction
22	0.0000	0.0175	0.1531	suction
23	0.0087	0.0135	0.1181	suction

transfer data. Point 11, at the trailing edge, is also deleted because it is not under the heat transfer foil.

#### 3.3.4 Pressure Measurements

On the surface of the blade, at the same chord locations as the thermocouples and at varying span locations near the 1/3 span point, there were 23 static pressure ports, see Table 1. The tunnel freestream total and static pressures were taken with a pitot-static tube located upstream of the cascade passage but downstream of the translating bars. Taking the pressure readings was a 36 port 36TS-1022 Scanivalve pressure transducer. Power for the pressure transducer and signal amplification was achieved through an Endevco model 109 power supply/model 106 conditioner unit set to 10.0 volts d.c. A Scanivalve CTRL2P/S2 solenoid controller allowed sequential stepping through the 36 ports and control from the HP2852A. Voltage readings from the pressure transducer were amplified in the conditioner and sent to the HP2852A integrating voltmeter through the multiplexer, and from there to the computer for storage. A linear calibration equation (where the slope is the change in pressure for a given change in voltage) converted the voltages from the Scanivlave pressure transducer into gage pressures in the data reduction phase of the experiment.

### 3.3.5 Velocity Measurements

Upstream velocity was determined using pressure found with a pitot-static tube stationed just downstream of the bars through the Scanivalve as described above and calculated using:

$$u_{\infty} = \left[ \frac{2 (P_0 - P_{static})}{\rho_{\infty}} \right]^{0.5} \quad (22)$$

Velocities throughout the cascade passage were also taken using a pitot-static tube. While this is not the best method of determining flow velocities, it is accurate as long as the probe is aligned with the flow direction (great care was taken to assure that this was the case). The probe was aligned with the oncoming flow by maximizing the total pressure. With the total pressure maximized, the total and static pressure measurements were recorded into the computer along with a manually input flow angle measured from the plane perpendicular to the "engine x-direction." These measurements were then used to determine the velocity in the x-direction needed for cascade flow characterization.

### 3.4 Software

Like most aspects of the hardware and data acquisition equipment used for this experiment, the software needed remained largely unchanged from the previous experiments of Gallasi (1989), Acree (1990), and Meschwitz (1991). All

programming was done in Microsoft QuickBASIC version 4.5 and is divided into three primary categories; calibration, data acquisition, and data reduction.

#### 3.4.1 Calibration Software

The only device needing calibration software was the Scanivalve pressure transducer. The program SCANCAL.bas was used to calibrate the pressure transducer. A series of pressures, both above and below atmospheric, was input to the Scanivalve and to one side of a U-tube manometer (filled with distilled water and yellow indicating fluid,  $\rho_{fluid} = \rho_{H2O}$ ). Atmospheric pressure was the reference for both systems. The computer recorded the pressure voltages from the transducer while the user input the pressure, in inches of water, from the U-tube. The hydrostatic equation was used to convert the input value from inches of water to gage pressure. After 20 or more different readings spanning the range of pressures encountered in this experiment, the data was plotted using Grapher and a best linear fit was made to the data. The equation of the line was then taken as the Scanivalve calibration equation and used in data reduction to convert pressure transducer voltages to gage pressures.

#### 3.4.2 Data Acquisition Software

A single program, ACQUIRE3.bas, was used to acquire all data for quantification wake passing effects on the heat

transfer in a turbine cascade. Largely this program remained unchanged from that existing from previous TCTF experiments, ACQUIRE.bas. The primary subroutines used were TEMPACQ.bas and PRESSACQ.bas. Additionally, a new program was written to accomplish the acquisition of velocity data, ISOBAR6.bas.

TEMPACQ was used to read and process the 30 thermocouple readings. When activated, TEMPACQ interrupted the power to the heat transfer surface via a relay channel in the HP2852A, to keep a power surge from going through the thermocouple wires and damaging the system. It then commanded the HP2853A to read the thermocouple voltages with the data acquisition unit's high-speed FET multiplexors. The HP2852A automatically converted the thermocouple readings into temperatures and transferred them to the PC for storage. To check the validity of the readings, they were then displayed to the screen. Using another program, HTXFER, discussed later, the data was reduced into heat transfer data.

PRESSACQ was used to gather the pressure transducer voltages for the 23 static ports on the blade and the upstream pitot-static tube through the Scanivalve. When activated, PRESSACQ commanded the HP2852A to sequentially march through 28 (not every port was utilized per the manufacturers instructions, see Table 2) of the Scanivalve's



Table 2 - Scanivalve Port Assignments

Port	Assignment
1	tap 1
2	tap 2
3	tap 3
4	tap 4
5	tap 5
6	tap 6
7	tap 7
8	tap 8
9	tap 9
10	tap 10
11	atmosphere
12	tap 11
13	tap 12
14	tap 13
15	tap 14
16	tap 15
17	tap 16
18	tap 17
19	tap 18
20	tap 19
21	tap 20
22	atmosphere
23	tap 21
24	tap 22
25	tap 23
26	pitot tube stagnation
27	atmosphere
28	pitot tube static

36 ports and record the output voltages. These voltages were then transferred to PC storage. Again, to check for validity, the pressure voltages were converted to coefficient of pressure values and plotted to the screen. Again, a separate program, PREDUCE, discussed in the following section, was used to reduce the pressure data for use in determining heat transfer data.

The only piece of software written exclusively for this experiment was ISOBAR6.bas. Since this experiment required the use of a pitot-static probe rather than an X-wire, previously existing programs, e.g., VELACQ.bas, and XWIRECAL.bas, could not be used. For each data point, ISOBAR6 would instruct the user to align the probe into the flow and command the HP2852A to gather the data as described previously. Unlike the other programs, ISOBAR6 accomplished the reduction of the output voltages into velocities using the Scanivalve's calibration coefficients and equation (20), rather than having a separate reduction program. The raw voltage data as well as the reduced data were then transferred to the PC for storage. Like the other data acquisition programs, ISOBAR6 displayed the velocity data to the screen to check for errors. The probe was relocated in the cascade passage to take the remaining velocity data points. A total of 35 data points were taken, seven equally spaced in each plane, in this manner for each test

condition.

A final program, TSET.bas, was used for real time display of temperature data. TSET commanded the HP2852A to read the five internal thermocouple values and transfer them to the PC for display in graphical form. TSET was used to determine when the temperatures in the turbine blade had come to an equilibrium. The internal thermocouples were read because reading them did not require the shutdown of the power supply to the heat transfer foil. A two second shutdown, approximately the length of time needed for the HP2852A to read the 23 outer thermocouples, would necessitate at least a five minute wait for equilibrium to be reached again. If readings were timed too close together, erroneous data would result.

Also, it is important to note that some of the heat energy within the blade is lost during the shutdown of the heat transfer foil. The average thermocouple will lose between 1 and 2 degrees Celsius during the shutdown. Fortunately, the last five thermocouples read are those along the blade's centerline, and they do not lose heat as readily as do the thermocouples under the heated foil. However, the unfortunate requirement to power down the foil does cause a slight impact on the heat transfer data.

### 3.4.3 Data Reduction Software

Data reduction software included two programs, HTXFER2.bas and PREDUCE.bas, both of which were unmodified from the programs used by Meschwitz (1991). HTXFER2 was used to reduce of the heat transfer data and PREDUCE reduced the blade and pitot-static data.

HTXFER2 took the blade and freestream recovery temperature data along with the blade static pressure data and calculated the local values for Reynolds number ( $Re_l$ ), convective heat transfer coefficient ( $h$ ), Nusselt number ( $Nu$ ), and turbulent and laminar theoretical Nusselt numbers for a flat plate and an arbitrary shape. The calculated values for the above were then sent to a file for permanent storage.

PREDUCE took the pressure transducer voltage data from the blade static ports and pitot-static tube and, with the calibration coefficients acquired in the Scanivalve calibration, converted the voltages to gage pressures. From the gage pressures the coefficient of pressure was calculated for each port on the blade and the freestream velocity of the tunnel was found from equation (20).

## IV RESULTS

### 4.1 General

As mentioned previously, this experiment studies the effect of wake passing on heat transfer. Among the parameters varied are freestream model Reynolds number and a number of bar conditions, e.g. bars out, bars installed, bars translating at different frequencies, and number of bars installed (183 vs. 92). For the purposes of this experiment the values for  $Re_\infty$  were approximately 227,400 for the low  $Re_\infty$  case and 303,200 for the high  $Re_\infty$  case. The cascade exit Reynolds numbers were  $Re_{exit} = 341,100$  and  $Re_{exit} = 454,800$ , calculated assuming  $u_{exit} = 1.5(u_\infty)$ , the typical velocity increase through this cascade. The bar passing frequencies are 80.3, 160.7, and 321.3 bars per second for the low, medium and high  $f_b$  values respectively. These frequencies correspond to bar speeds of 6.235, 12.469, and 24.938 m/s respectively.

### 4.2 Cascade Flow Characterization

#### 4.2.1 Blade Pressure Coefficient Characterization

For cascade passages that exhibit well-behaved flow the coefficient of pressure curves for different Reynolds numbers and data runs will coalesce. Such was the case for the TCTF with the new configuration, as seen in Figures 7 and 8. Both of the sets of curves display a great degree of

agreement between the data in that the curves for bars installed conditions take the same shape for both Reynolds number cases. Also, there are noticeable differences between the plots of bars installed cases and the bars out case, for both  $Re_{crit}$  cases, attributable to wake effects.

Figures 7 and 8 both show the coefficient of pressure reaching a value of nearly 1.0 at the stagnation point, tap 2 at  $s/c = -0.0087$  (see Figure 6 for approximate port locations), for the bars out case. This is another aspect of a well-behaved cascade's coefficient of pressure curve. For the set of curves depicting the bars installed cases,  $C_p$ 's do not quite reach unity at tap 2. Also, at tap 1,  $s/c = 0.0875$ , on the bars installed plots of Figures 7 and 8, the flow had not re-accelerated to freestream conditions yet as it had in the bars out condition. This may suggest a shift in the stagnation point toward tap 1. This possibility is discussed further in a later section. However, without a more dense packing of static pressure ports in the stagnation region, there is no way of being certain. Overall, these coefficient of pressure curves indicate a well-behaved flow. A further discussion of the coefficient of pressure curves is given in Section 4.4.1, where in depth analysis of the effects of wake passing is done.

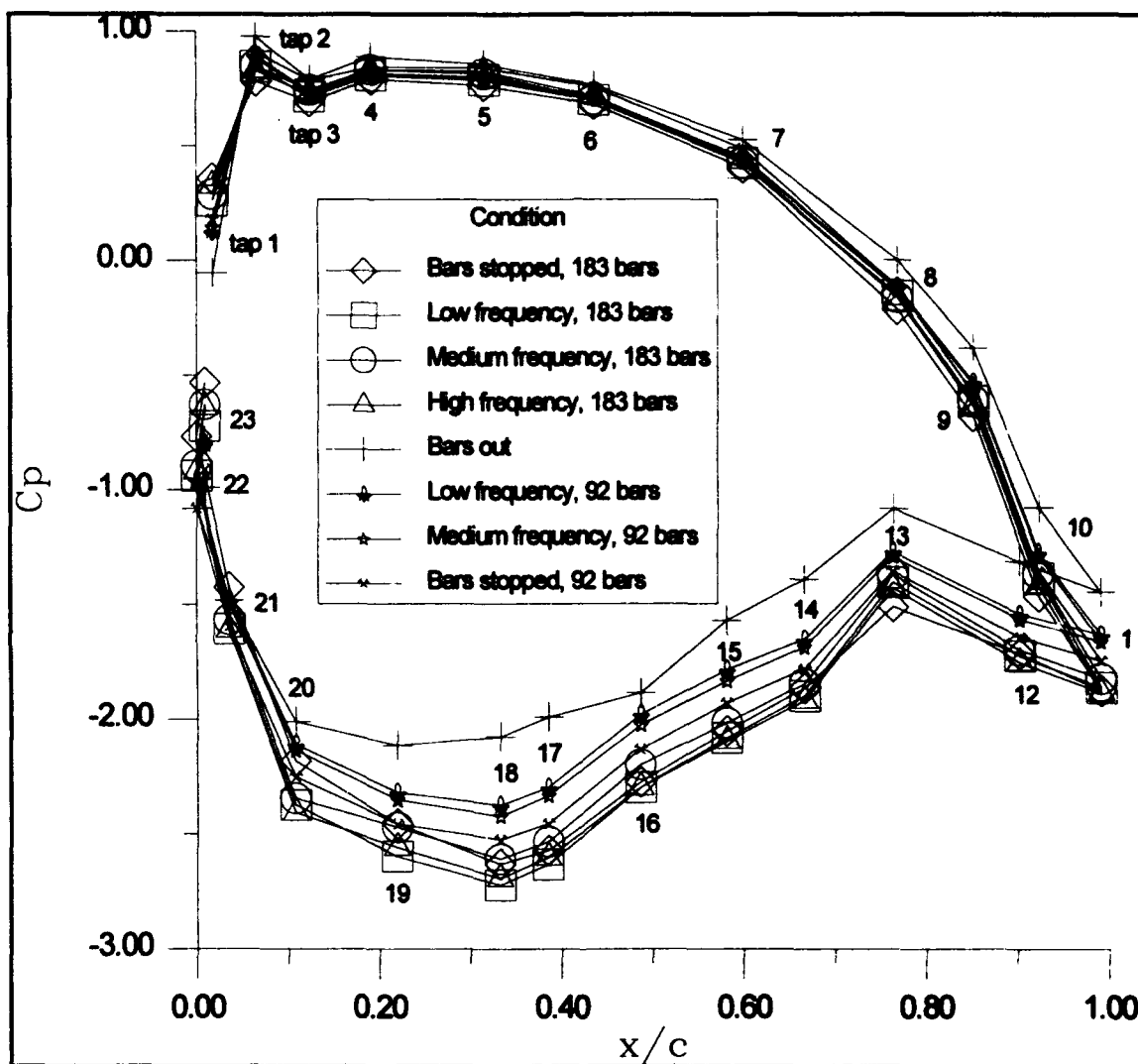


**Figure 7** - Coefficient of pressure curves  
for  $Re_{exit} = 341,100$ .

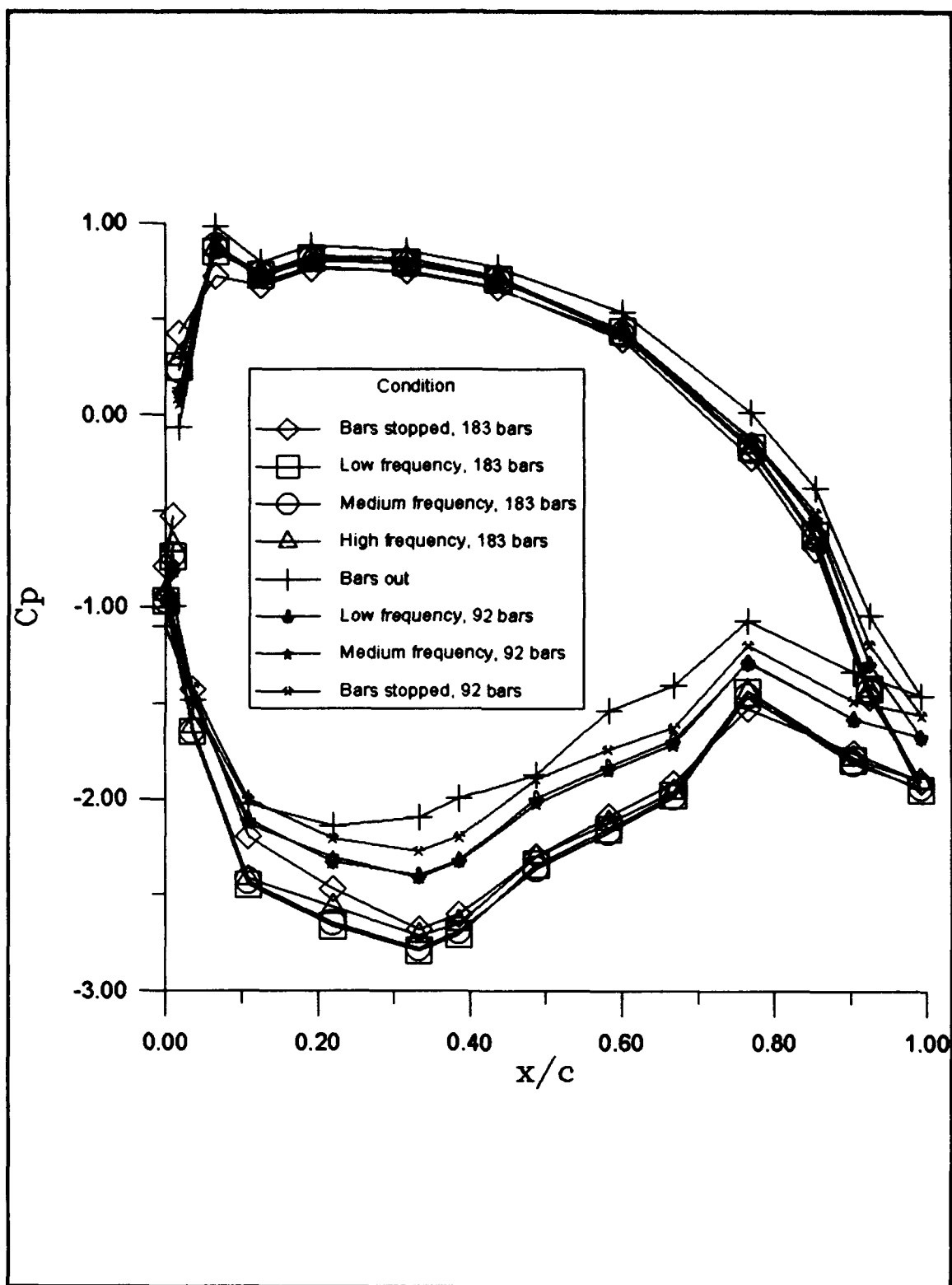


Figure 8 - Coefficient of pressure curves for  $Re_{exit} = 454,800$ .



#### 4.2.2 Cascade Passage Velocity Characterization

Using a pitot-static probe, as described in Chapter III, velocities and flow angles were taken along the cascade centerline in five planes in the cascade passage. The velocities and angles were condensed into  $U_x$ , the component of velocity in the x or "through engine" direction. A well behaved cascade passage will exhibit a smooth change in flow speed from the pressure surface of one blade to the suction surface of the next. On a plot of  $U_x$  versus passage location this would exhibit itself in a truncated sinusoidal curve with lower  $U_x$  at the pressure surface and higher near the suction surface. This is the case with Figures 9-18. A plot of the measured flow angles across the cascade passage is also included for information, Figures 19-28. These plots are not used to characterize the cascade flow.

Lack of access to the entire width of the first plane precluded an examination of the periodicity of the cascade's entry flow. However, the data given for the cascade passage flow more than adequately characterizes the flow as well behaved and able to be compared to the results of previous cascade experiments.

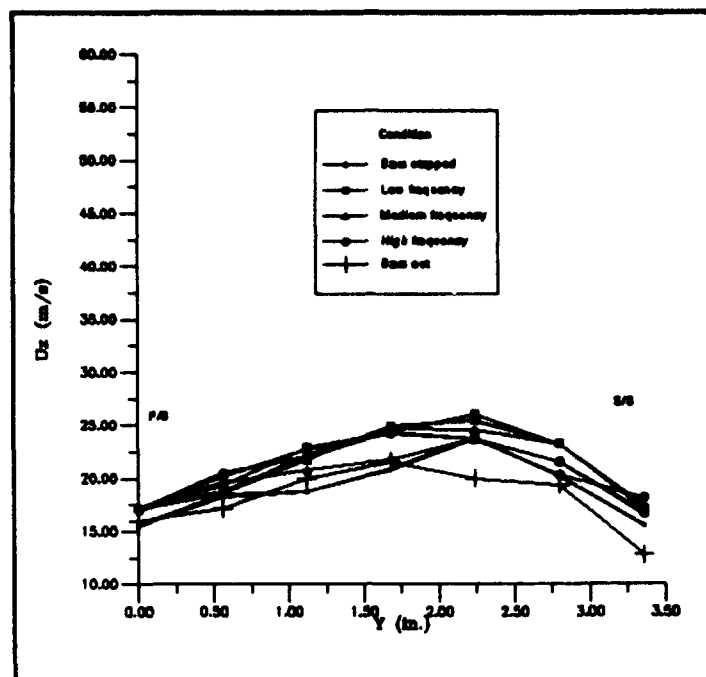


Figure 9 - Plane 1  $U_x$ 's  
 $Re_{exit} = 341,100$ .

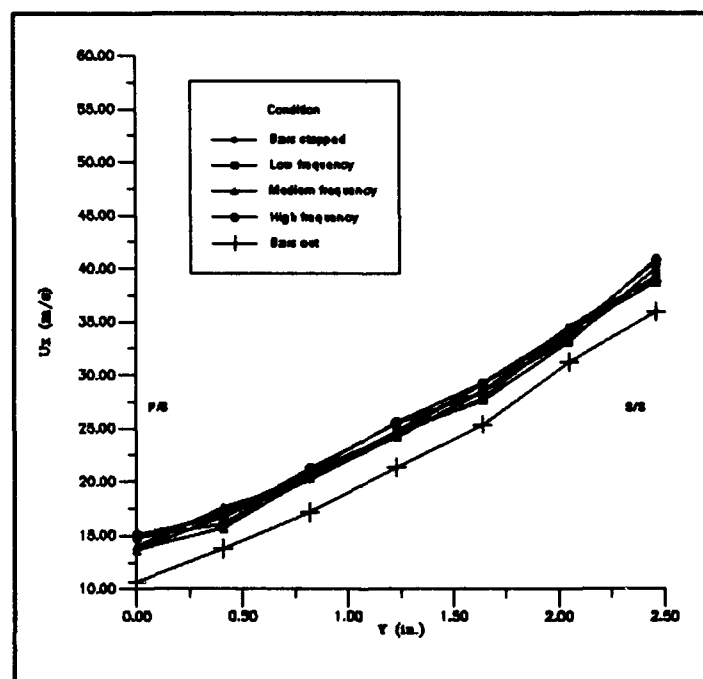


Figure 10 - Plane 2  $U_x$ 's  
 $Re_{exit} = 341,100$ .

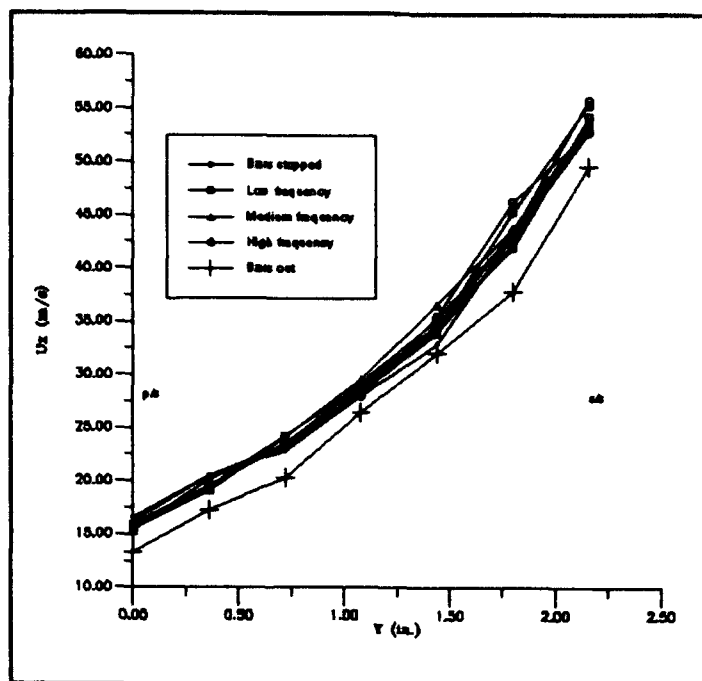


Figure 11 - Plane 3  $U_x$ 's  
 $Re_{exit} = 341,100$ .

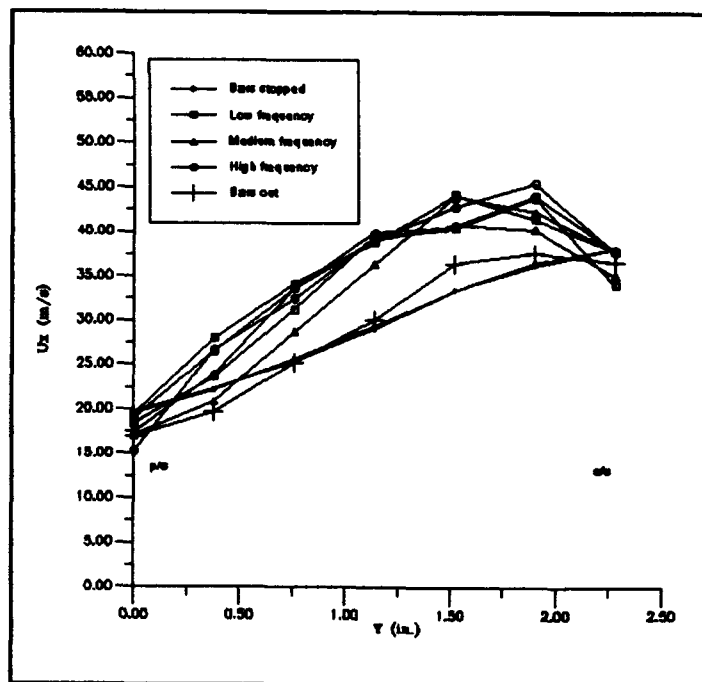


Figure 12 - Plane 4  $U_x$ 's  
 $Re_{exit} = 341,100$ .

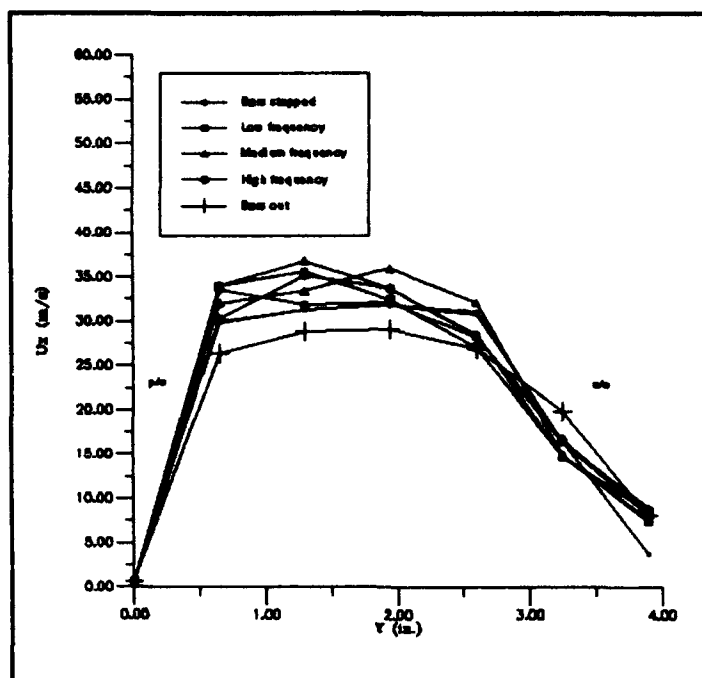


Figure 13 - Plane 5  $U_x$ 's  
 $Re_{exit} = 341,100$ .

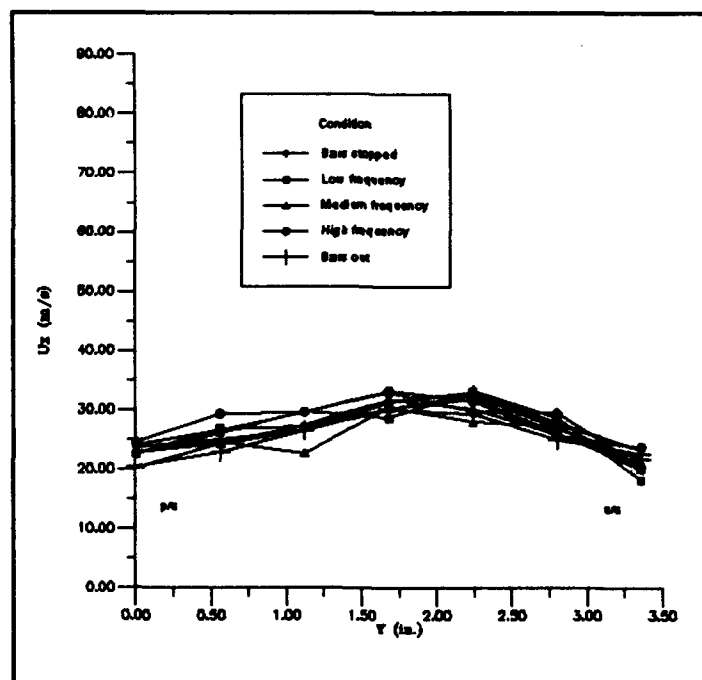


Figure 14 - Plane 1  $U_x$ 's  
 $Re_{exit} = 454,800$ .

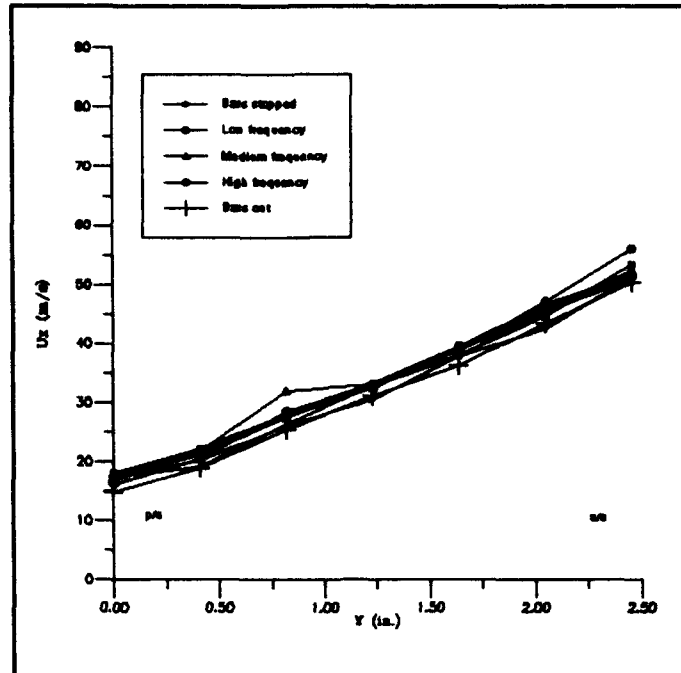


Figure 15 - Plane 2  $U_x$ 's  
 $Re_{exit} = 454,800$ .

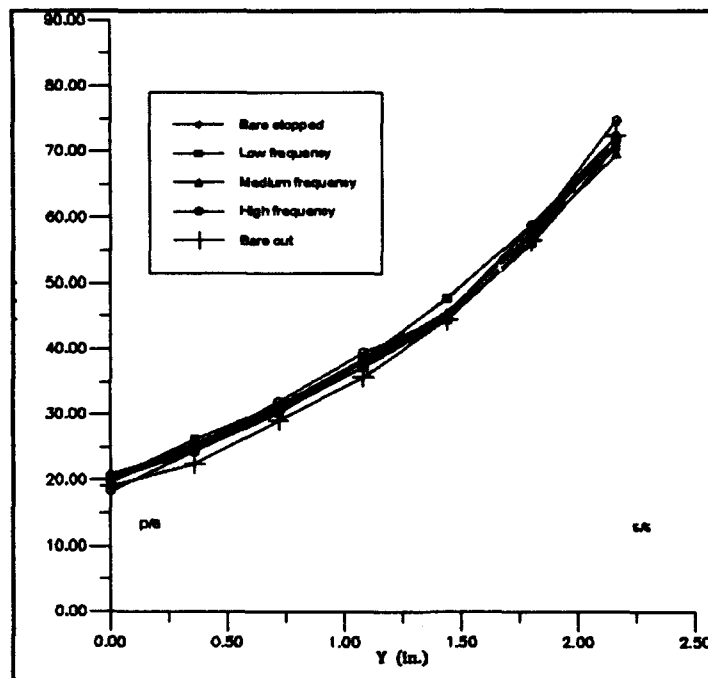


Figure 16 - Plane 3  $U_x$ 's  
 $Re_{exit} = 454,800$ .

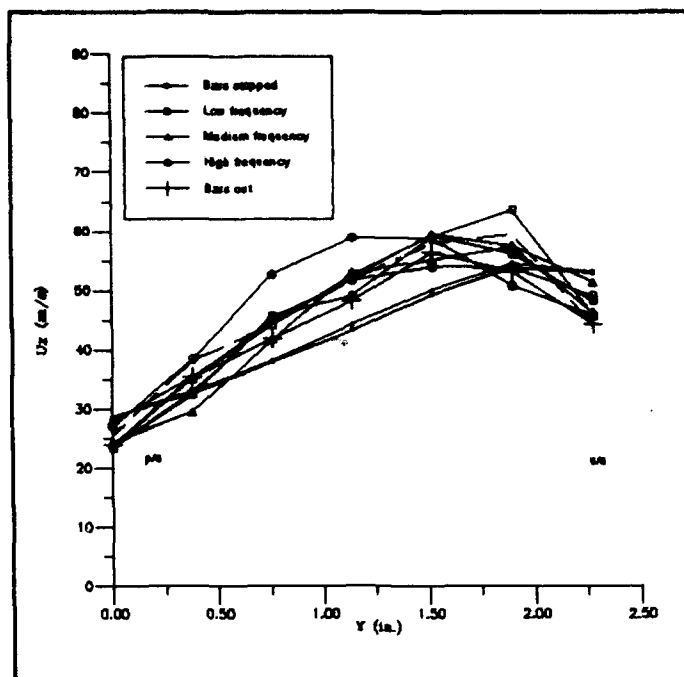


Figure 17 - Plane 4  $U_x$ 's  
 $Re_{exit} = 454,800$ .

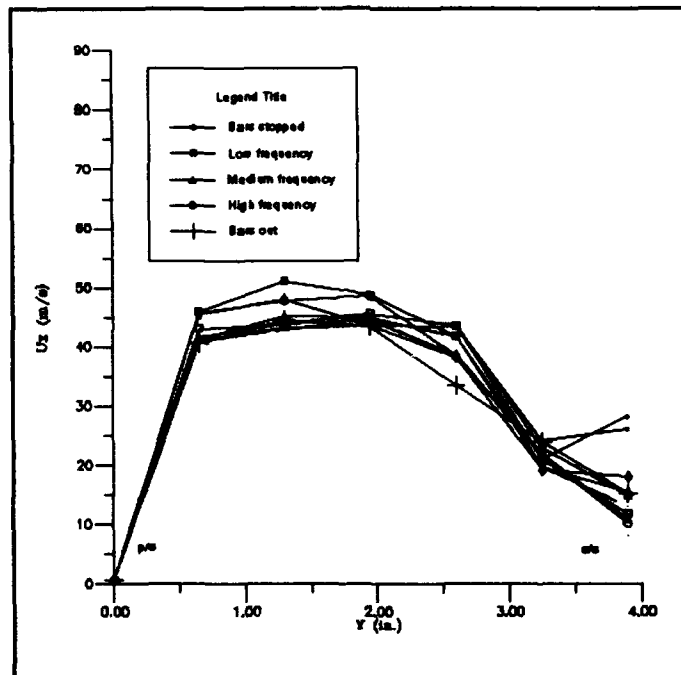


Figure 18 - Plane 5  $U_x$ 's  
 $Re_{exit} = 454,800$ .

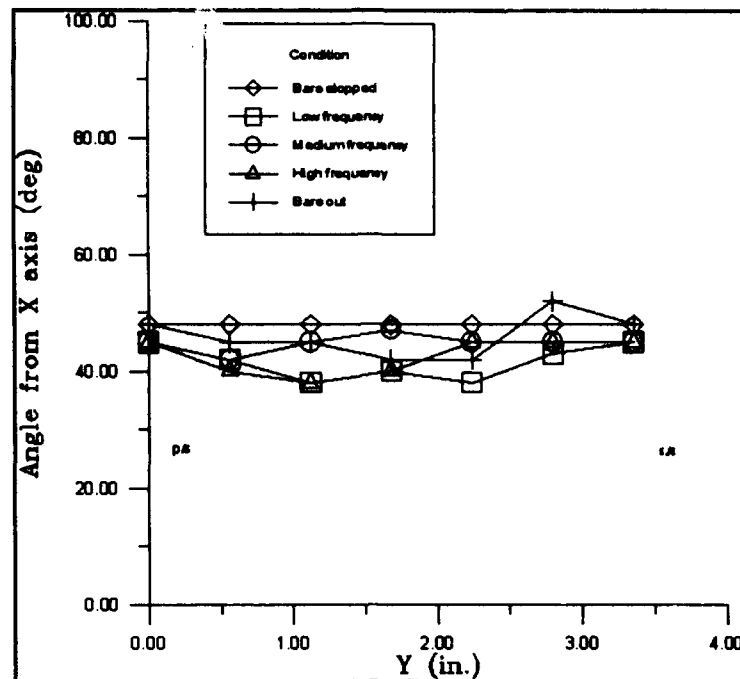


Figure 19 - Plane 1 angles  
 $Re_{exit} = 341,100$ .

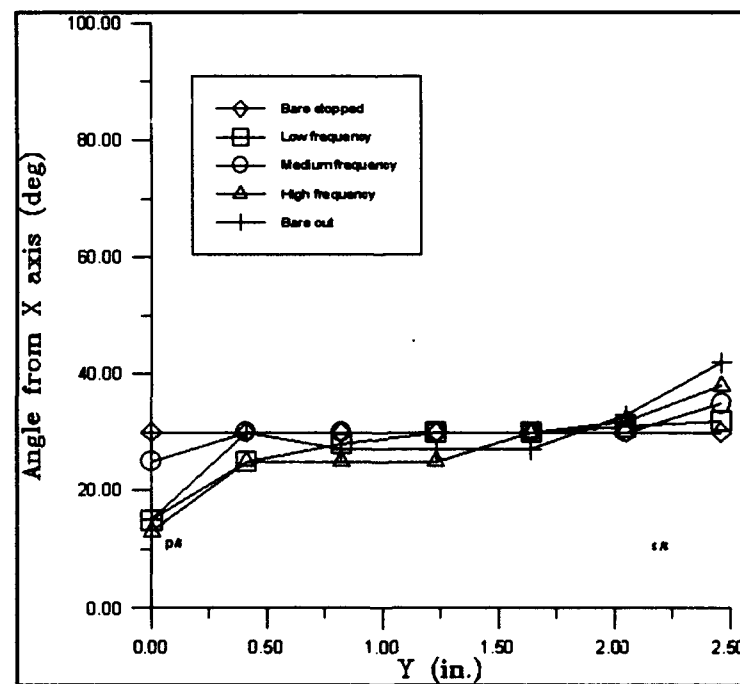


Figure 20 - Plane 2 angles  
 $Re_{exit} = 341,100$ .

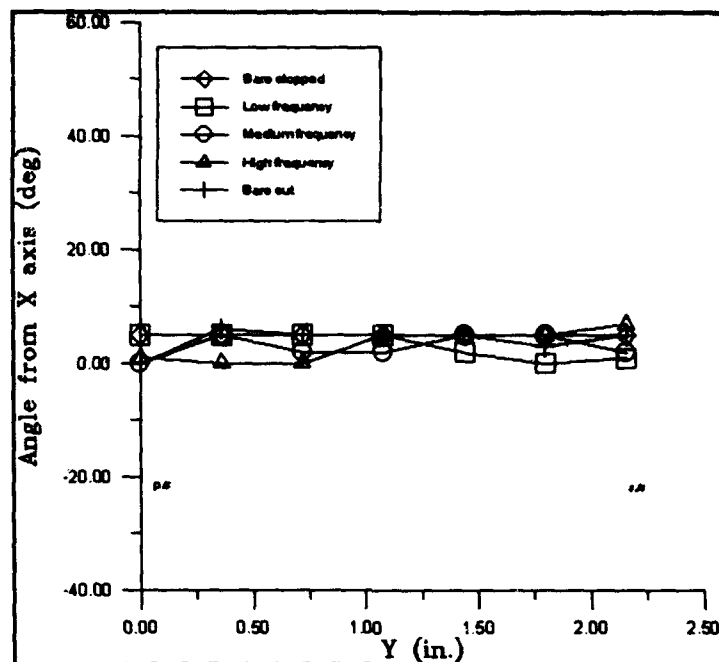


Figure 21 - Plane 3 angles  
 $Re_{exit} = 341,100.$

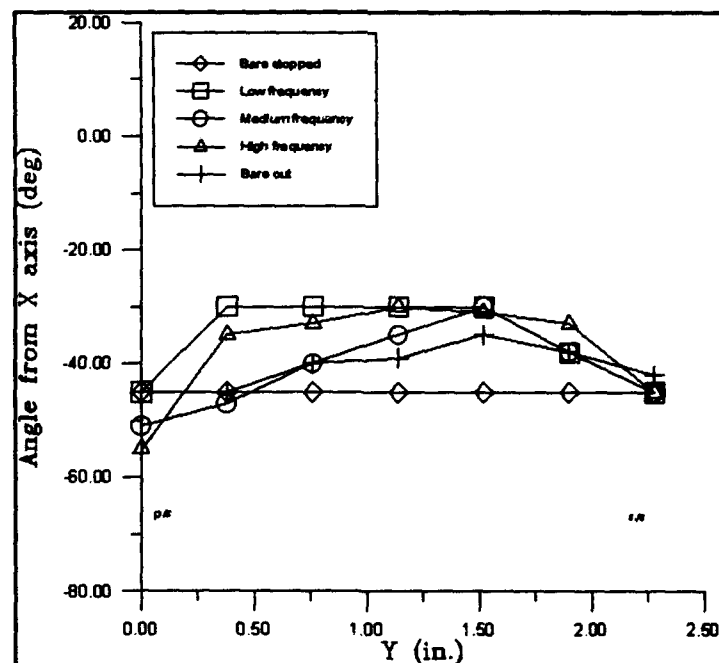


Figure 22 - Plane 4 angles  
 $Re_{exit} = 341,100.$



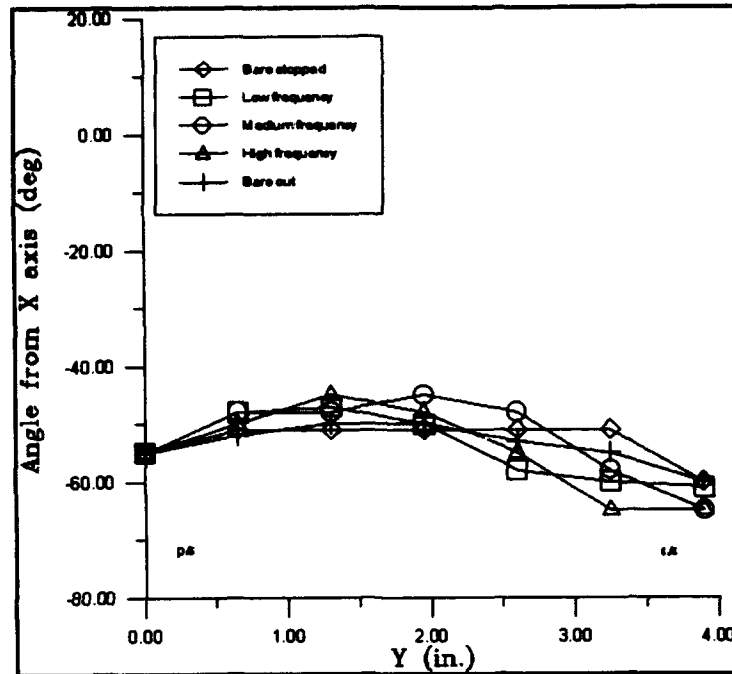


Figure 23 - Plane 5 angles  
 $Re_{exit} = 341,100$ .

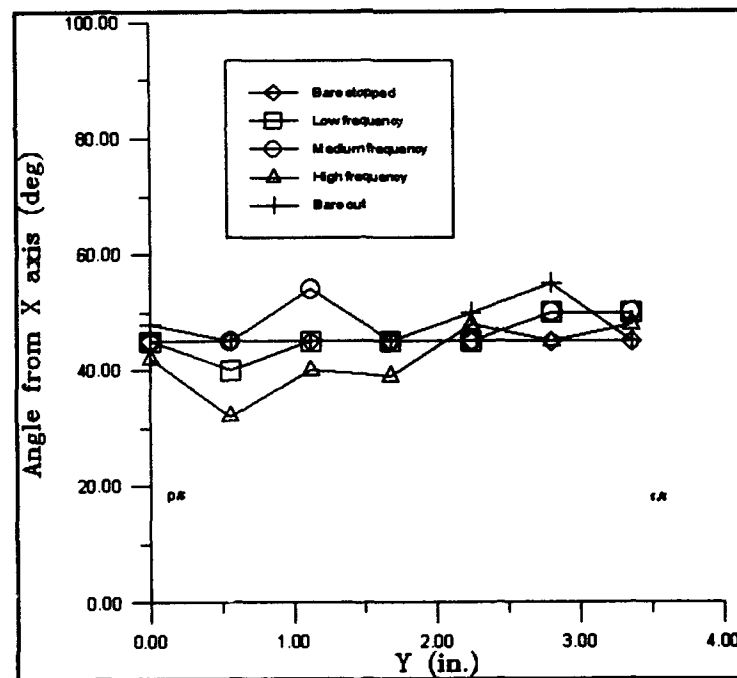


Figure 24 - Plane 1 angles  
 $Re_{exit} = 454,800$ .

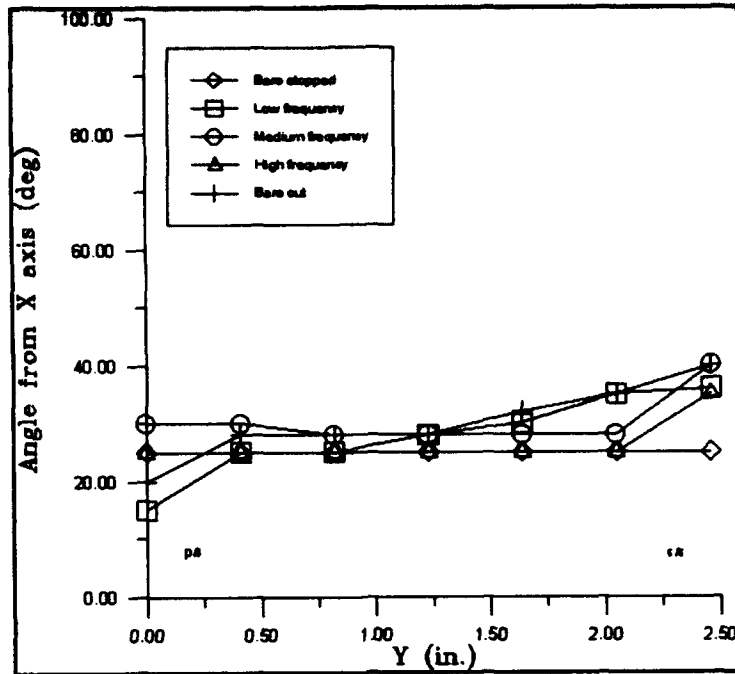


Figure 25 - Plane 2 angles  
 $Re_{exit} = 454,800$ .

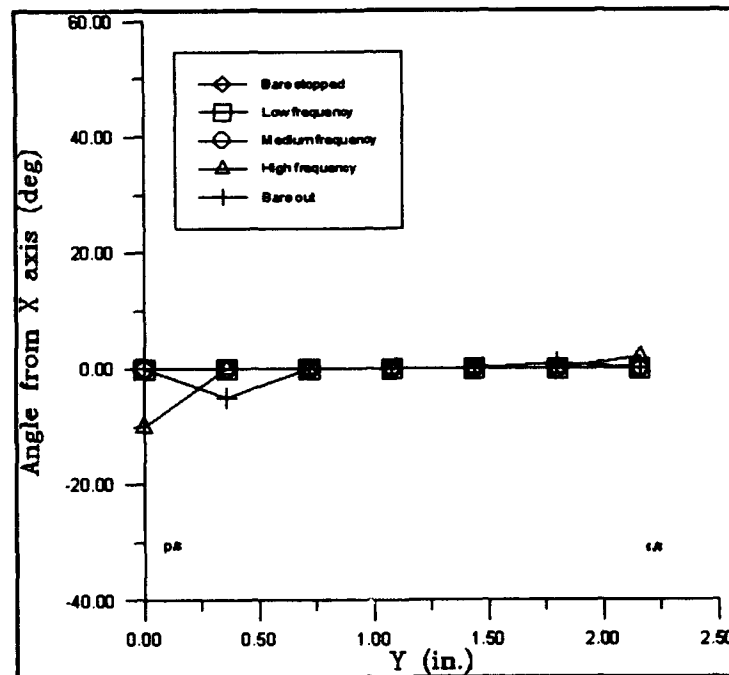


Figure 26 - Plane 3 angles  
 $Re_{exit} = 454,800$ .

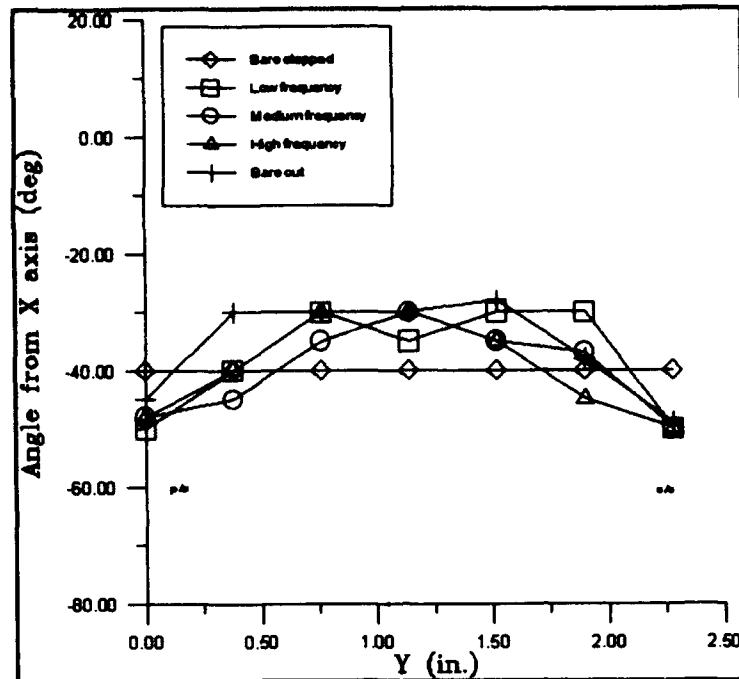


Figure 27 - Plane 4 angles  
 $Re_{exit} = 454,800$ .

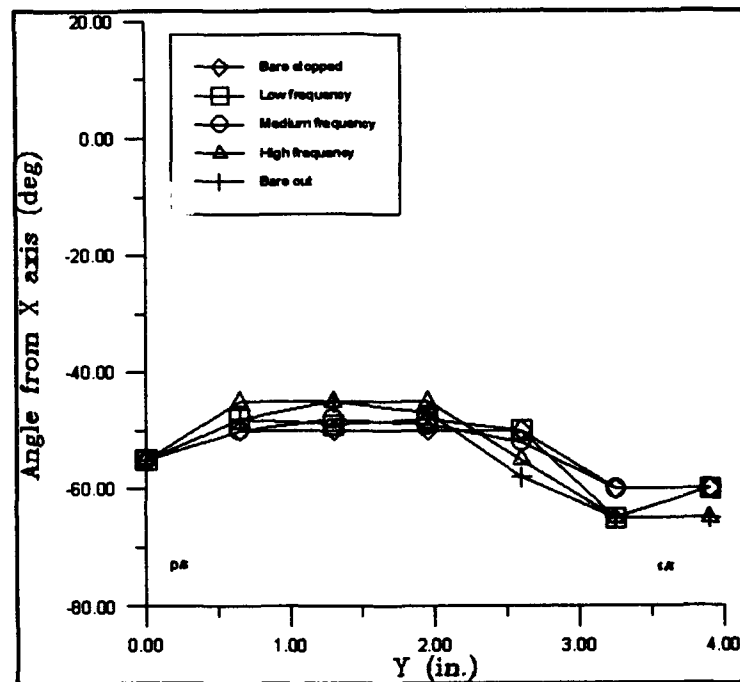
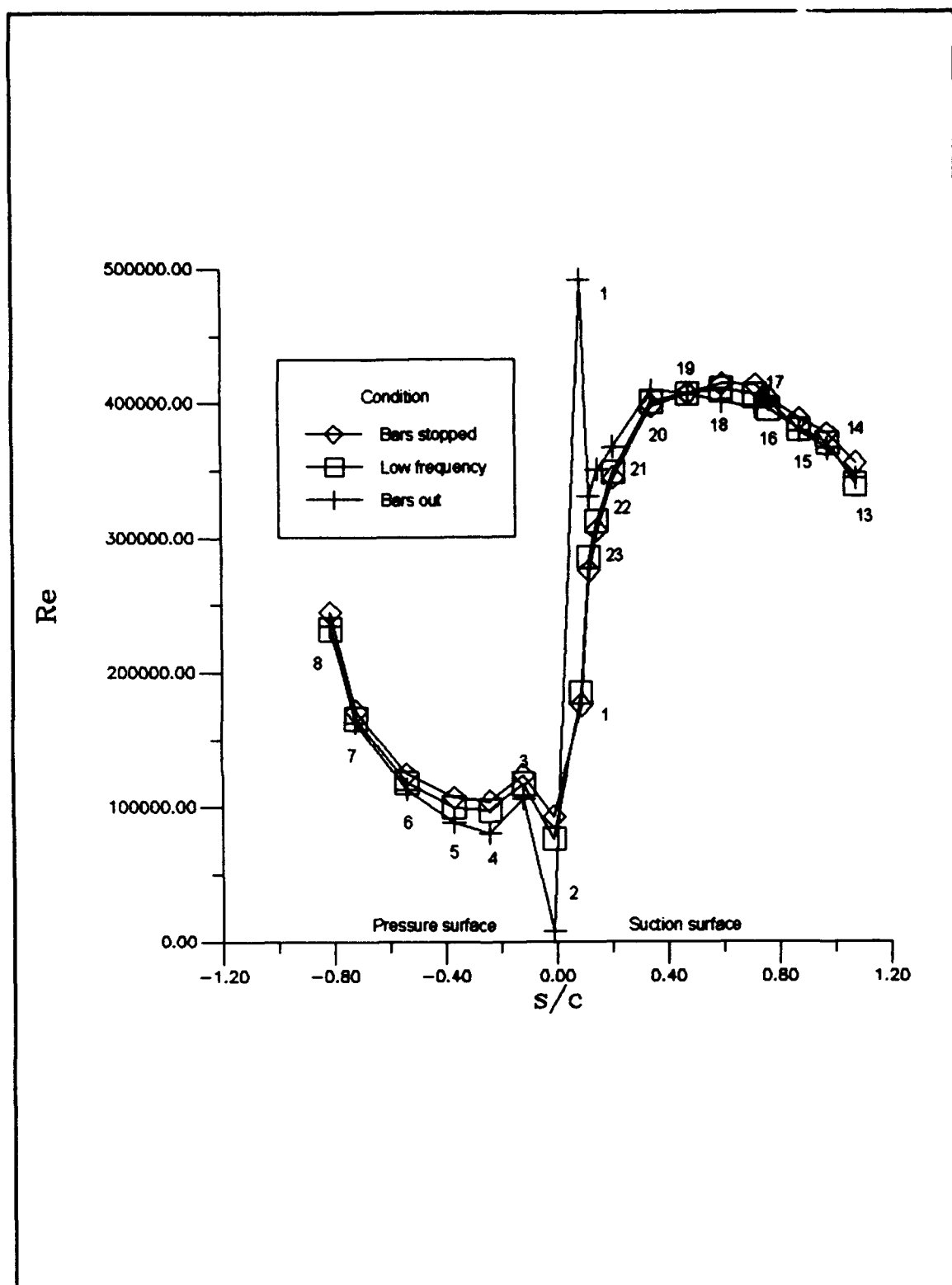


Figure 28 - Plane 5 angles  
 $Re_{exit} = 454,800$ .

#### 4.2.3 Local Blade Velocity Characterization

Figure 29 depicts the  $Re_k$  versus blade surface location for  $Re_{exit} = 341,100$ . By choosing to define the Reynolds number in this way, the effect is a comparison of local velocities along the blade surface. The plot shows that the lowest velocity on the blade's surface is at tap two, as expected from the coefficient of pressure plots. Along the suction side of the blade there is a dramatic acceleration near the leading edge followed by a region of deceleration due to the adverse pressure gradient on the blade. On the pressure surface there is an acceleration of the flow between ports two and three followed by a slight deceleration, perhaps due to separation, and then the flow reaccelerates to match the conditions on the suction surface at the trailing edge. All these factors suggest a well behaved and repeatable cascade flow.

However, the most interesting feature of Figure 29 is the difference between the two bars installed cases and the bars out case at taps 1 and 2. For the bars out case it is obvious that tap 2 is the stagnation point because  $Re_k$  is so low here. On the other hand, the value of  $Re_k$  for the bars installed cases is much greater at tap 2. This indicates that the stagnation point has shifted to some degree. The differences between the tap 1 data for the bars out versus the bars installed data is discussed in a later section.



**Figure 29** - Local chord based Reynolds number over the surface of the blade,  $Re_{exit} = 341,100$ .

#### 4.2.4 Effects of the Forward Bar Guide

Due to the installation of the guide shown in Figure 4 in front of the cascade passage, it was necessary to determine the effect it had on the cascade passage flow. At the time of this experimental work, another experiment (Braunschneider, 1993) was also being conducted on the TCTF to determine the total pressure loss coefficients through the cascade passage due to wake effects. Figure 30 is a topographical plot of the total pressure loss coefficients through the height of the cascade in plane #2,  $x/c = 0.26$ , with the bar guide installed. At the top of the cascade passage there is a dense grouping of loss lines owing to the vortices that typically develop in cascades at the end walls. However, at the bottom of the cascade, downstream of the forward bar guide, the losses are not as great. This showed that the development of the end wall vortices was inhibited by the forward bar guide.

Another point to be made from Figure 30 is that in the center of the cascade passage there were relatively few losses. This indicated that the center of the passage was free of three dimensional effects. It was for this reason that the heat transfer foil, thermocouples and pressure taps were located in the center of the instrumented blade.

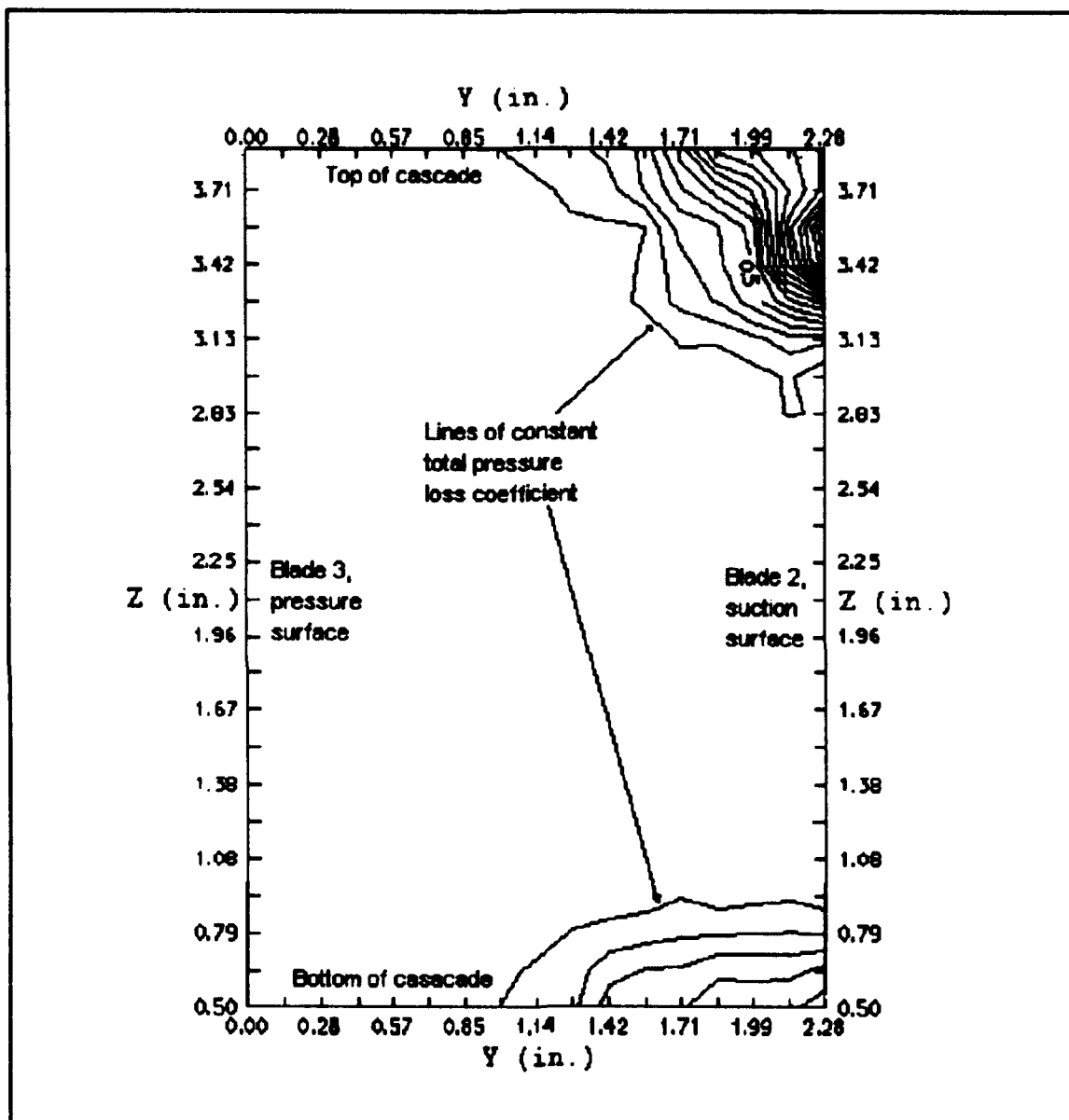


**Figure 30** - Topographical Plot of total pressure loss coefficient, plane 2,  $Re_{ext} = 341,100$ .

### 4.3 Test Plan

After the preliminary work (e.g., equipment testing and calibration, cascade characterization, etc.) was done, the actual testing took the form of the test matrix shown in Table 3. The conditions were as described in section 4.1. It was not feasible to go beyond these values for the testing due to the limitations on the flow speed through the test section and the stability of the belt and bars. At the lower frequencies it was difficult to match the exact bar passing frequency for each run. The differences were slight, however, and in the range of  $\pm 3\%$ .

The results of the tests performed are presented and analyzed in the following sections. In addition, suggestions for making improvements to the setup of the experiment, and hardware and software used, and for further experimental testing are offered in Chapter V.



Table 3 - Test Plan

Test Condition						
Re <sub>∞</sub>		Bar Condition				
Low Re <sub>∞</sub>	Medium Re <sub>∞</sub>	Out	Stopped	Low f <sub>b</sub>	Medium f <sub>b</sub>	High f <sub>b</sub>
X		X				
X			X			
X				X		
X					X	
X						X
	X	X				
	X		X			
	X			X		
	X				X	
	x					x
Half (92) Bars Installed Cases						
X			X			
X				X		
X					X	
	X		X			
	X			X		
	X				X	

#### 4.4 Effects of Wake Passing

As already seen in the differences between Figures 7 and 8, and discussed in section 4.2.1, the existence of bars upstream of the cascade passage and the passing of wakes across the cascade blades influences the blade's coefficient of pressure. The following sections will explore this cause/effect relationship in greater detail and discuss the effects on heat transfer in the blade.

##### 4.4.1 Turbine Cascade Blade Coefficient of Pressure

Figures 7 and 8 are the coefficient of pressure curves for each of the two  $Re_\infty$  cases run during this experiment ( $3.03 \times 10^5$ , and  $2.27 \times 10^5$ ), and all of the bar conditions. Every condition has some differences compared to the others. Otherwise the study of one frequency would be sufficient. The differences between the bars out condition, the 92 bars installed cases, and the 183 bars installed conditions are discussed in the following sections.

Effects of 183 Bars Installed. The reason that the bars out condition differs from the other conditions was the effects of the wakes and their associated turbulence. The freestream turbulence induced by the wakes has influenced the blade's boundary layer and allowed the flow over the blade to remain attached longer. This accelerated the flow to a higher velocity at the trailing edge as evidenced by a lower coefficient of pressure at the trailing edge of the

bars installed cases.

There is also a small, but discernible, difference between the bars stopped condition and the remaining conditions with the bars translating, for the 183 bars installed cases. The differences between the bars stopped condition and the bars translating conditions were a result of an immobile wake impinging on the same location of the blade in the bars stopped case where in the bars translating cases the wakes would convect down the surface of the blade. In other words, the bars stopped case created local regions of velocity deficit across the blade's surface where the bars translating cases did not. This velocity deficit showed up as a higher value of the  $C_p$ 's for the bars stopped cases in some areas.

More interesting though was the noticeable difference between the various conditions near the leading edge of the suction surface in the low  $Re_{\text{exit}}$  case. Specifically, the large scattering of leading edge, tap 2,  $C_p$ 's. Doorly (1984) found that a small separation bubble existed intermittently very near the leading edge of the suction surface. While Doorly's cascade was not of the same design as the TCTF it is possible that the cascade blades were both experiencing a separation. Another possible reason could be the shifting of the stagnation region. Either the existence of a separation bubble near the suction surface leading edge

or the shifting of the stagnation region would explain these differences, but, more testing would need to be done to verify if either, or both, take place on the blade.

Effect of 92 Bars Installed. The effect of removing half of the bars, from 183 to 92 bars, was to diminish the effect of the wakes on the coefficient of pressure curves for the blade. The 92 bars installed cases lie between the bars out case and the 183 bars installed cases. This indicates that less wake turbulence is produced in the 92 bars installed cases than the 183 bars installed cases. As a result the flow over the blade's suction surface is not accelerated to as high a velocity, seen as higher  $C_p$ 's on the suction surface. Also, since the lower two bar passing frequencies of the 183 bars installed cases were matched, this indicates that the coefficient of pressure is not frequency dependent for these conditions.

There are also noticeable differences between the bars stopped cases and the bars translating cases for both  $Re_{exit}$  conditions on the suction surface. For the lower exit Reynolds number case the value of  $C_p$  is lower with the bars stopped than with the bars translating, indicating a higher velocity over the suction surface. For the medium exit Reynolds number this relationship flips, with the bars translating cases having the lower values of coefficient of pressure.

Most likely the differences between the bars stopped and the bars translating cases are a result of the position of the stationary bar with respect to the blade. In the low exit Reynolds number case the stationary bars were in a location with respect to the blade that allowed the wake from the bars to aid the boundary layer in remaining attached. This resulted in a higher suction surface velocity. For the medium  $Re_{exit}$  case the stationary bars' locations hindered the boundary layer and induced it to separate earlier. This resulted in a lower blade suction surface velocity. More testing in this area would be required to confirm the effects of the different stationary bar locations.

The Importance of  $C_p$  Curves. The reason differences in  $C_p$  curves are so important is that the heat transfer in the blade is highly dependent on the local blade velocity and the condition of the boundary layer, be it laminar or turbulent (Kays, et al., 1993). The  $C_p$  curves were a valuable aid in the analysis of the velocity and boundary layer. Judging from the curves, the most dramatic changes in heat transfer will come as a result of the bars being present, with some changes coming as a result of the bars translating at some frequency rather than remaining in one place.

Considering the curves and the large variance in  $C_p$  on the suction surface between the bars out and bars in cases, one might be tempted to conclude that the suction side will have the greater change in heat transfer when comparing the various conditions. This was not be the case though. The suction surface  $C_p$ 's are far more sensitive to disturbances than the pressure surface. The fact that the pressure side shows a small amount of difference in the  $C_p$  at all is indication that the heat transfer in this area will change.

#### 4.4.2 Turbine Cascade Blade Heat Transfer

There are many methods of characterizing the heat transfer in a body. Among these methods are convection heat transfer coefficient ( $h$ ), Nusselt number ( $Nu$ ), Stanton number ( $St$ ), and normalized Nusselt number ( $Nu/Re^{1/2}$ ), also called the Frössling number. All of the methods boil down to the same thing, heat transfer. Which is preferred is often a matter of choice. However, there are strengths and weaknesses to each method. Each method may highlight a different aspect of the flow and heat transfer. Also, empirical relationships exist for a few of the methods and they will be taken advantage of in the analysis. In the following sections each of these methods will be utilized and the results of each will be analyzed.

Convection Heat Transfer Coefficient ( $h$ ). Figures 31 and 32 are plots of  $h$  along the blade surface. As expected

the increase of freestream velocity ( $Re_\infty$ ) produced an increase in the heat transfer in both the bars installed and the bars out cases. This is expected as the greater the volume of air moving through the cascade the greater the air's ability to absorb heat energy per time.

Also expected was the difference between the bars installed and bars out cases. The increase from bars out to bars installed is seen throughout the blade's surface excepting the suction surface trailing edge. It is toward the trailing edge that the suction surface boundary layer transitions from laminar to turbulent and may even separate. The higher heat transfer associated with a turbulent boundary layer allows the heat transfer rate of the bars out condition to match that of the bars installed conditions, which have a turbulent boundary layer to begin with, at the trailing edge. Similar results were found in experimental works by Dullenkopf, et al. (1990) and Schultz, et al. (1986).

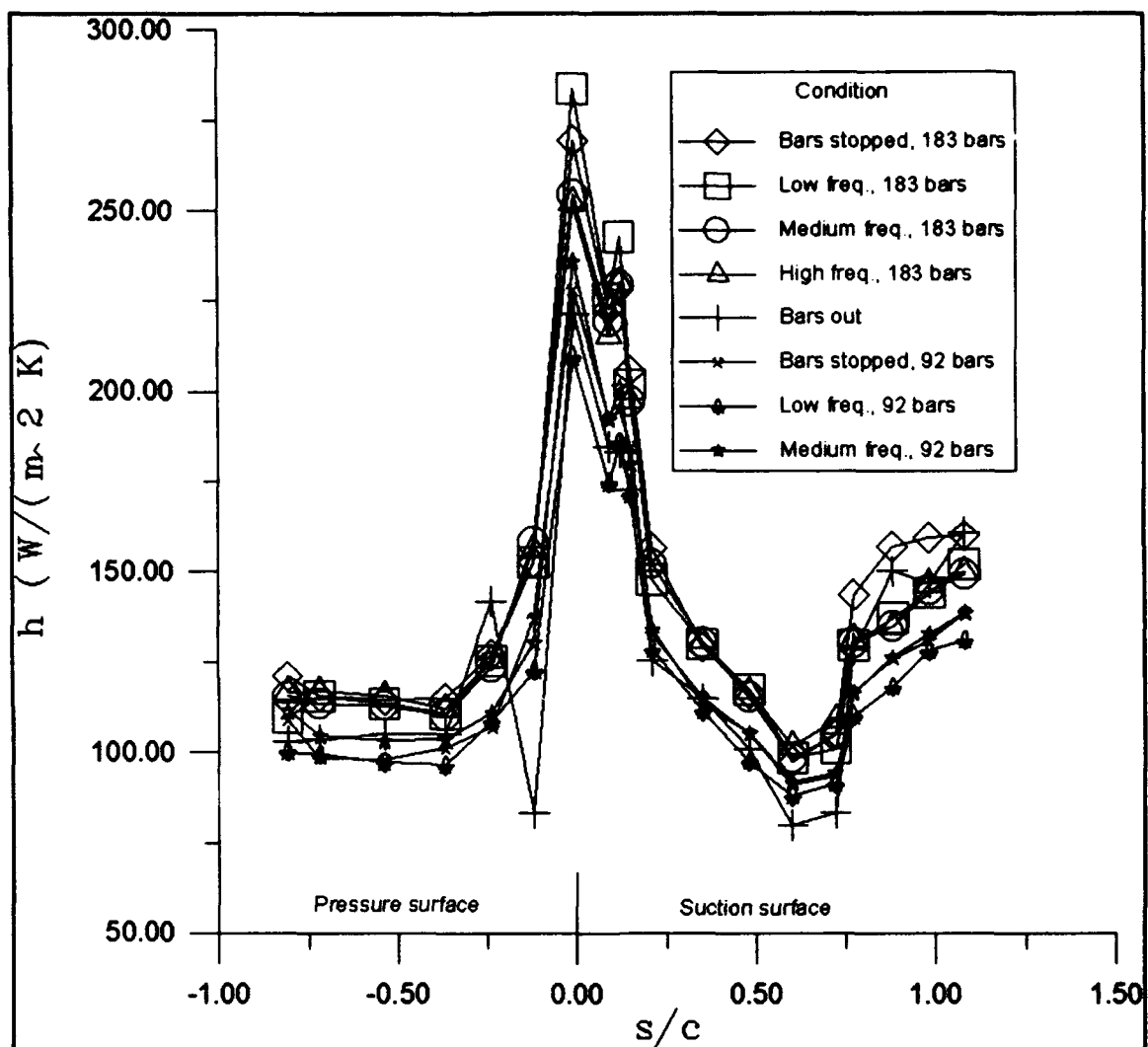
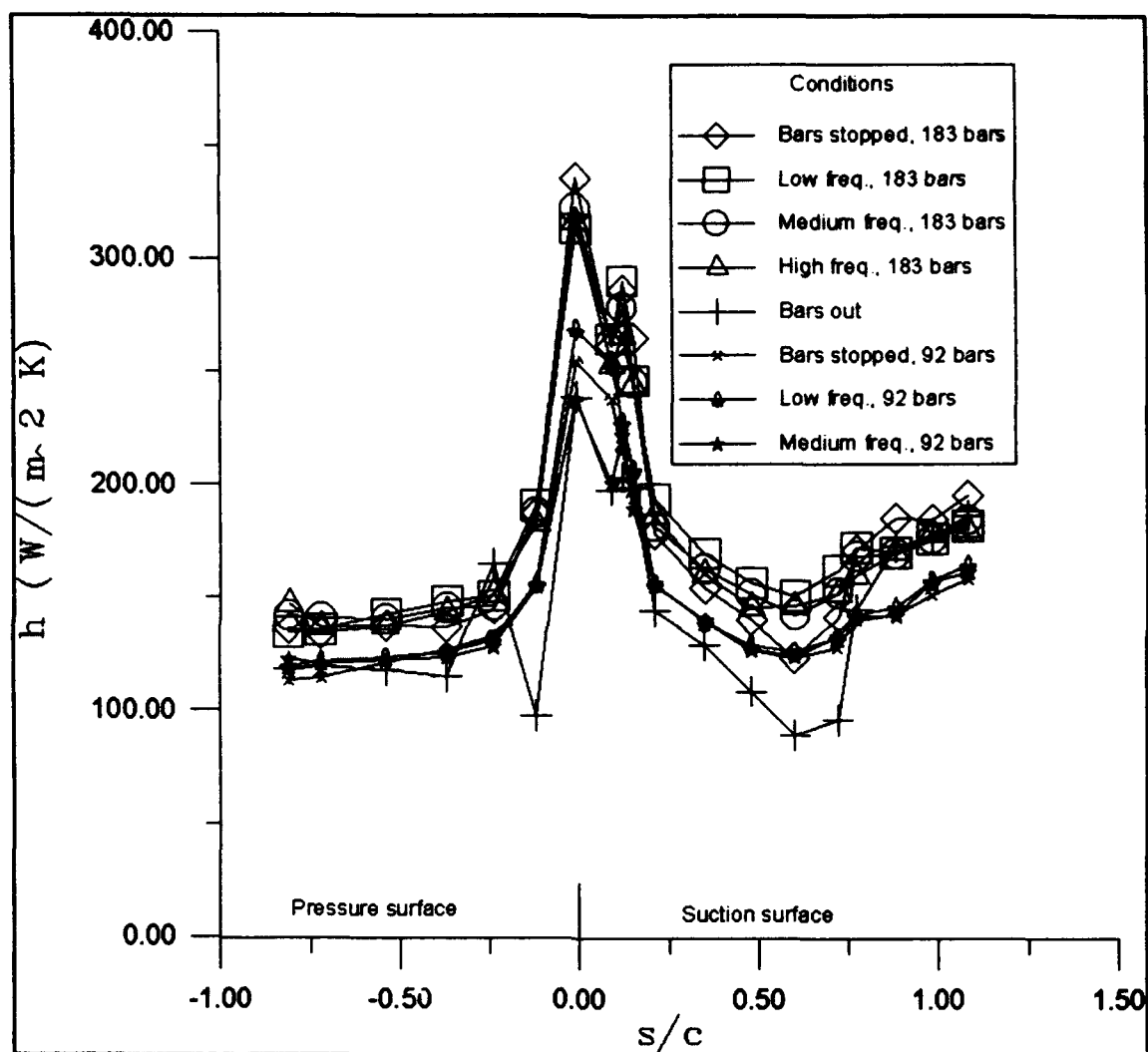


Figure 31 - Convective heat transfer coefficient ( $h$ ) over the surface of the blade,  $Re_{exit} = 341,100$ .





**Figure 32** - Convective heat transfer coefficient ( $h$ ) over the surface of the blade,  $Re_{exit} = 454,800$ .

A unusual event occurs, with the bars out, on the pressure surface at points 3 and 4,  $s/c = -0.1199$  and  $-0.2450$ , where  $h$  is very low at 3 and then jumps above the bars installed cases at point 4 in Figures 31 and 32. This is due to a local region of separation of the boundary layer when the bars are not present that is prevented when the bars are installed. The local region of separation was confirmed by oil drop experiments by Meschwitz (1991), for low freestream turbulence.

Some small differences can be detected between the bars installed cases also outside the stagnation region,  $s/c = -0.1199$  to  $0.0875$ . The bars stopped case has slightly higher values for heat transfer at the trailing edge of the suction surface at low  $Re_{exit}$ . However, repeatability studies showed that this increase was not consistent and can therefore be attributed to experimental uncertainties.

In the stagnation region of the blade, especially for the low  $Re_{\infty}$  case, there are large variances in  $h$ . Doorly (1984) shewed that the passing of wakes caused the stagnation point of the blade to vary around a mean location during a single test. In this experiment this type of behavior was exhibited also in Figures 7, 8 and 29. With the stagnation point shifting depending on the frequency with which the blade's leading edge is struck by a wake, the associated heat transfer at the leading edge varied.

Nusselt Number (Nu). Figures 33 and 34 show the local Nusselt number over the surface of the blade. Like the convective heat transfer coefficient plots, the largest change in  $Nu$ , for like Reynolds numbers, is seen between the bars out and bars installed cases. For all of the bars installed cases, regardless of frequency, the curves appear to coalesce.

As with all of the plots before, like conditions tend to have the same curve shape for both Reynolds numbers. In other words, the values for  $Nu$  change due to Reynolds number changes but the relationship from one point to the next is maintained between the two Reynolds numbers.

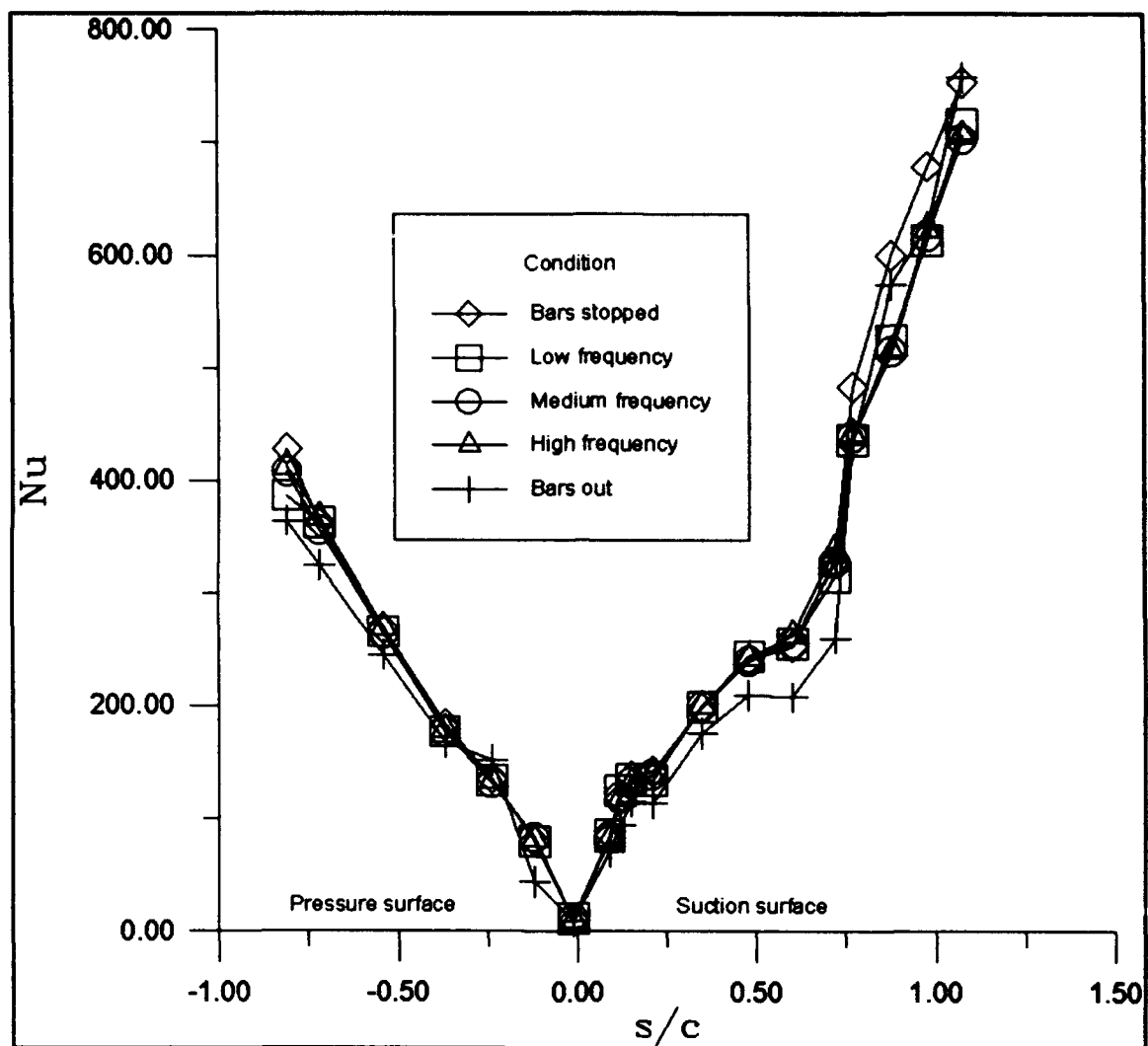


Figure 33 - Local Nusselt number over the surface of the blade,  $Re_{exit} = 341,100$ .

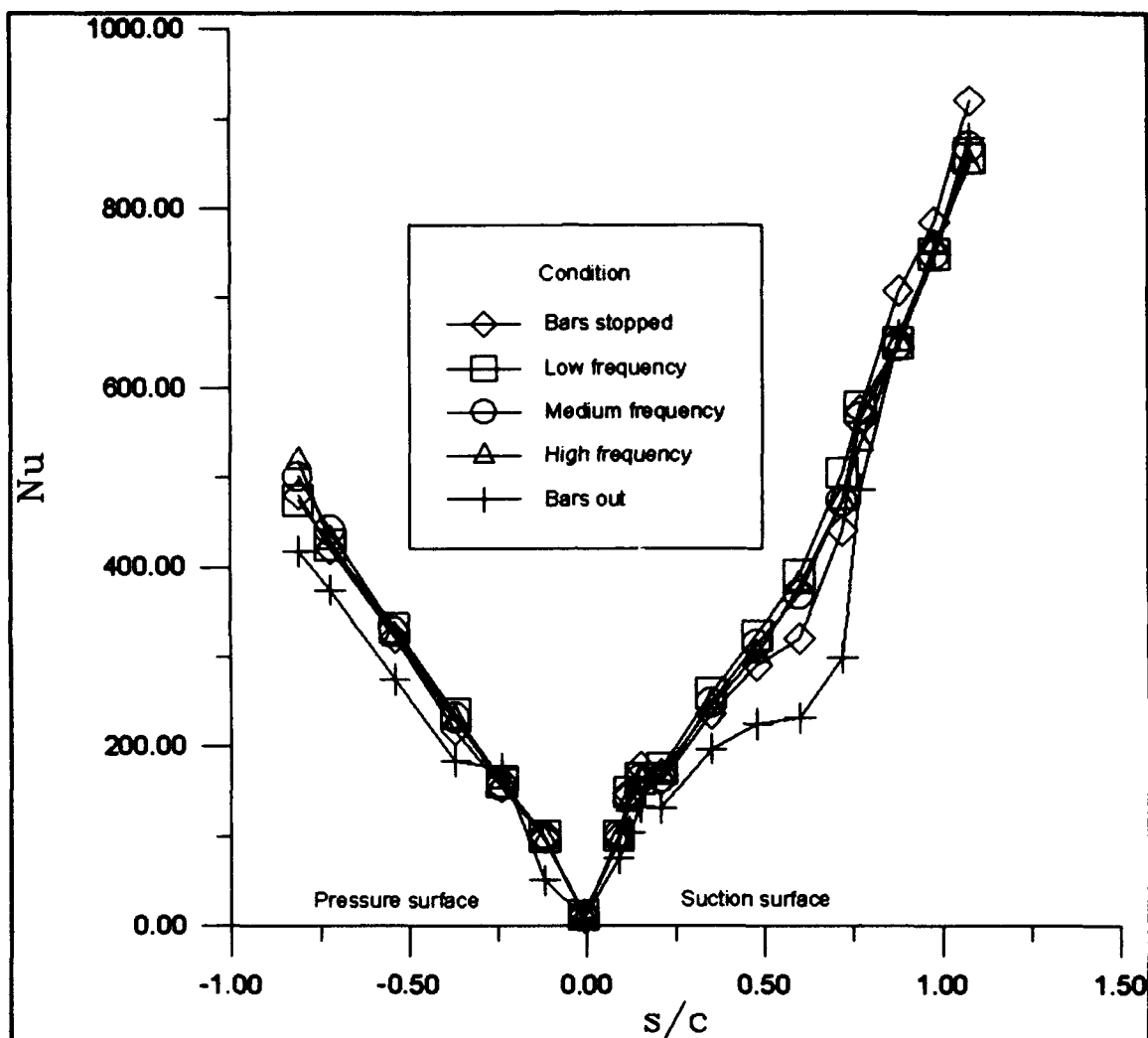
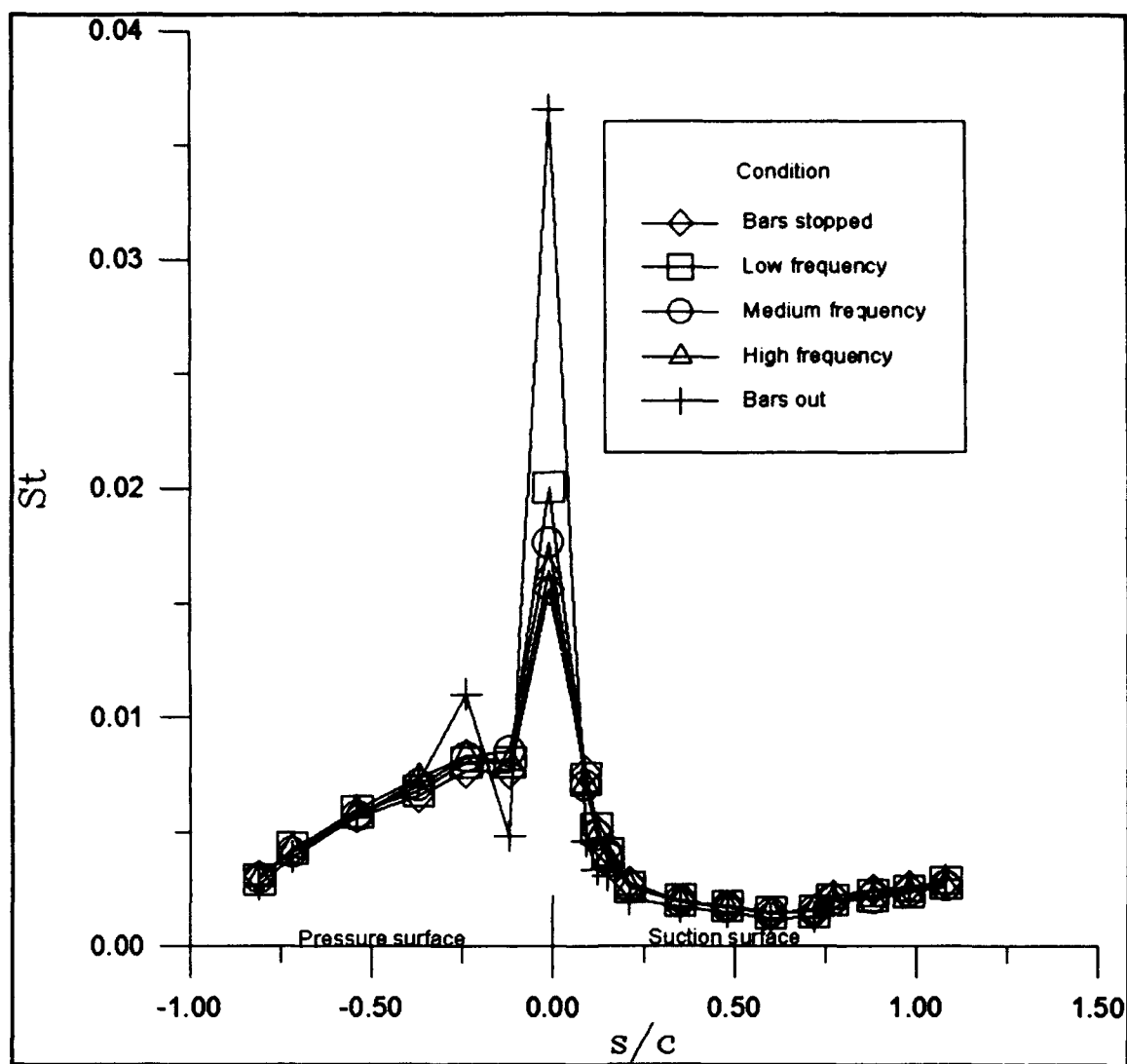


Figure 34 - Local Nusselt number over the surface of the blade,  $Re_{exit} = 454,800$ .

Stanton Number ( $St$ ). The effect of plotting the local Stanton number over the blade surface is an interesting one (Figures 35 and 36). The Stanton number, because of the way it is defined (dividing the local Nusselt number by the local  $Re$ ), tends to exaggerate the differences between the various cases at the stagnation point because  $Re_s$  is low. Elsewhere it brings the curves together. This characteristic of the  $St$  curves highlights well the effect of wake passing at the stagnation point, a decrease in heat transfer. The differences are most notable between the bars out and bars installed cases. This is most likely again the result of a shifting stagnation region due to wake passing.

The other interesting aspect of the  $St$  curves is the difference between the bars out and bars installed cases at points 3 and 4,  $s/c = -0.1199$  and  $-0.2450$ . The value of  $St$  point 3 is well below that of 4, with  $St$  at 4 being higher than the values for the bars installed cases. This was also seen in the  $h$  curves, Figures 31 and 32.



**Figure 35** - Local Stanton number over the surface of the blade,  $Re_{exit} = 341,100$ .

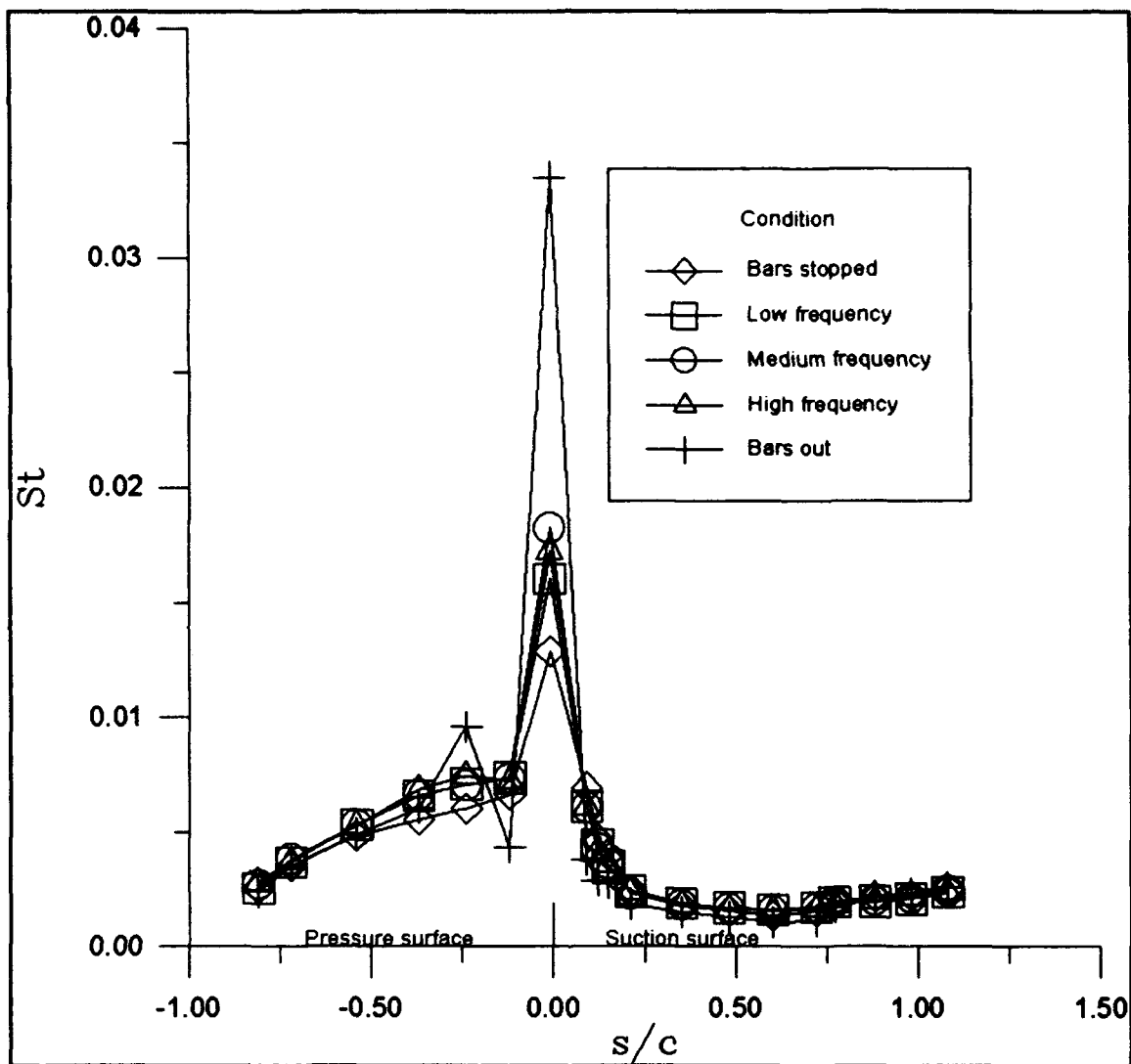


Figure 36 - Local Stanton number over the surface of the blade,  $Re_{exit} = 454,800$ .



Frössling Number. The final method of depicting the heat transfer in the turbine cascade blade is the Frössling, or normalized local Nusselt, number defined by:

$$Fr = \frac{Nu_i}{Re_i^2} \quad (23)$$

Figures 37 and 38 are plots of the Frössling number over the surface of the blade. Again a different method of depicting the heat transfer has brought out a new characteristic that the other methods minimized. In this instance it is the heat transfer near the mid-chord on the pressure surface for the bars stopped, medium  $Re_c$  condition. This result is most likely attributed to the effect of a constant non-translating wake impinging on the blade and creating a velocity deficit, as mentioned earlier. The suction surfaces of both Reynolds numbers show the same dramatic increase in heat transfer due to bar installation as the other plots. All other aspects of the plot are the same as those seen in the previous plots, as well. For comparison, Kays (1993) shows that for a laminar flat plate  $Fr = 0.295$  and for a turbulent flat plate  $Fr = 0.0296Re_i^{0.3}Pr^{1/3}$ . The turbulent flat plate values would range from 0.417 at  $Re_i = 10,000$  to 1.347 at  $Re_i = 500,000$ .

Figure 39 is another plot of Frössling number plotted against the bar passing Strouhal number ( $S_b$ ) and only for the geometric stagnation point, point 2,  $s/c = -0.0087$ . In

this instance the Frössling number is calculated from the Nusselt number based on true chord,  $Nu_c$ , and  $Re_\infty$ .

The stagnation point Frössling numbers for the bars out and low bar passing frequency cases went against intuition in that they are lower for a higher  $Re_\infty$ . This is most likely due to the uncertainty of the data. However, the general trend in the data is interesting because it shows a relatively constant geometric stagnation point heat transfer for increasing bar passing frequency. Kays (1993) also shows a value for stagnation point  $Fr = 0.702$ , where both  $Nu$  and  $Re$  are based on the blunt nosed radius of a body. This radius in the TCTF is 5mm. However, the Frössling number was not defined in this manner for Fig. 39.

Figure 40 uses the same data as Figure 39 but divides by the bars out Frössling number to show the percentage increase in heat transfer.

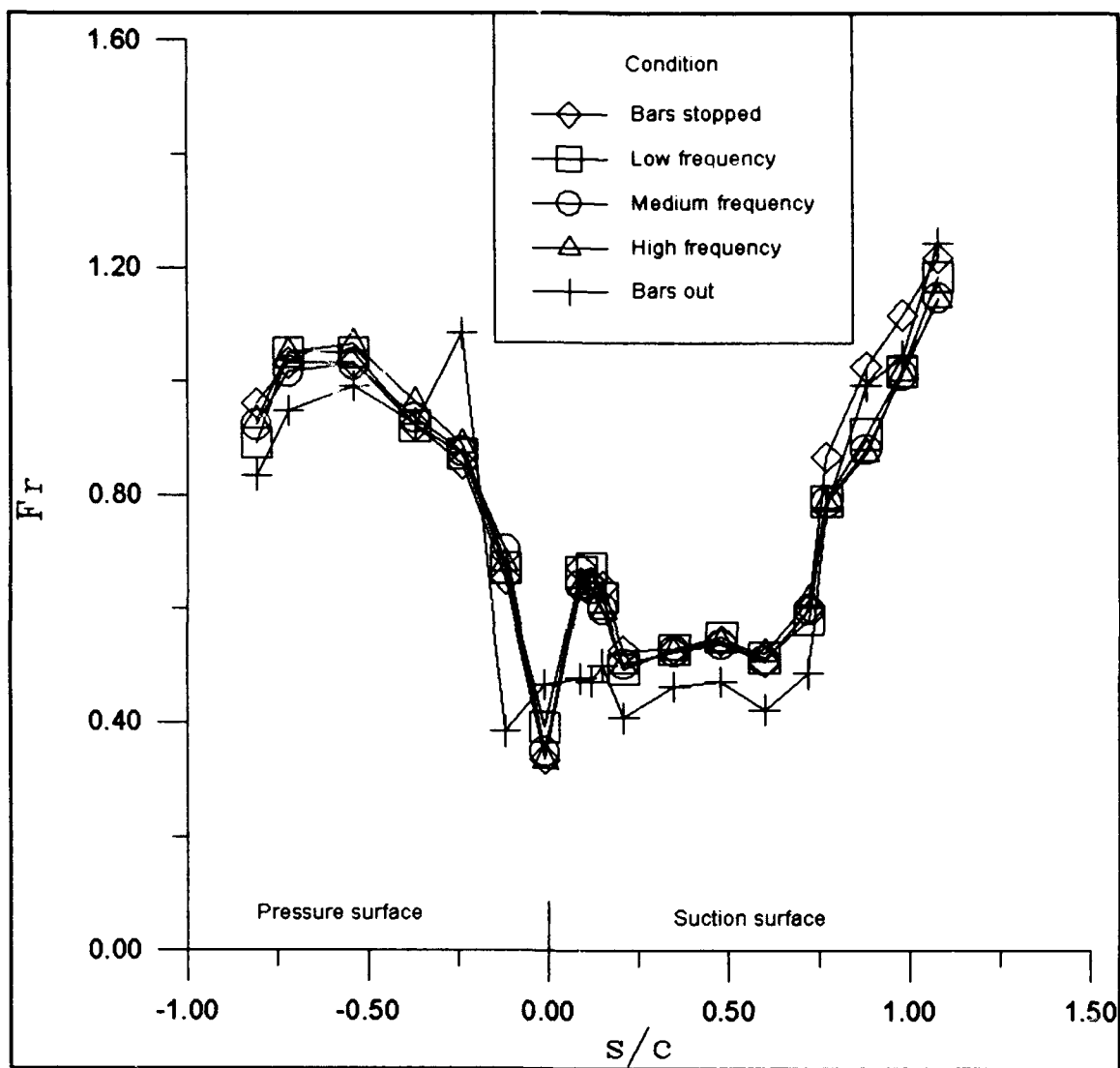


Figure 37 - Local Frösslings number over the surface of the blade,  $Re_{exit} = 341,100$ .

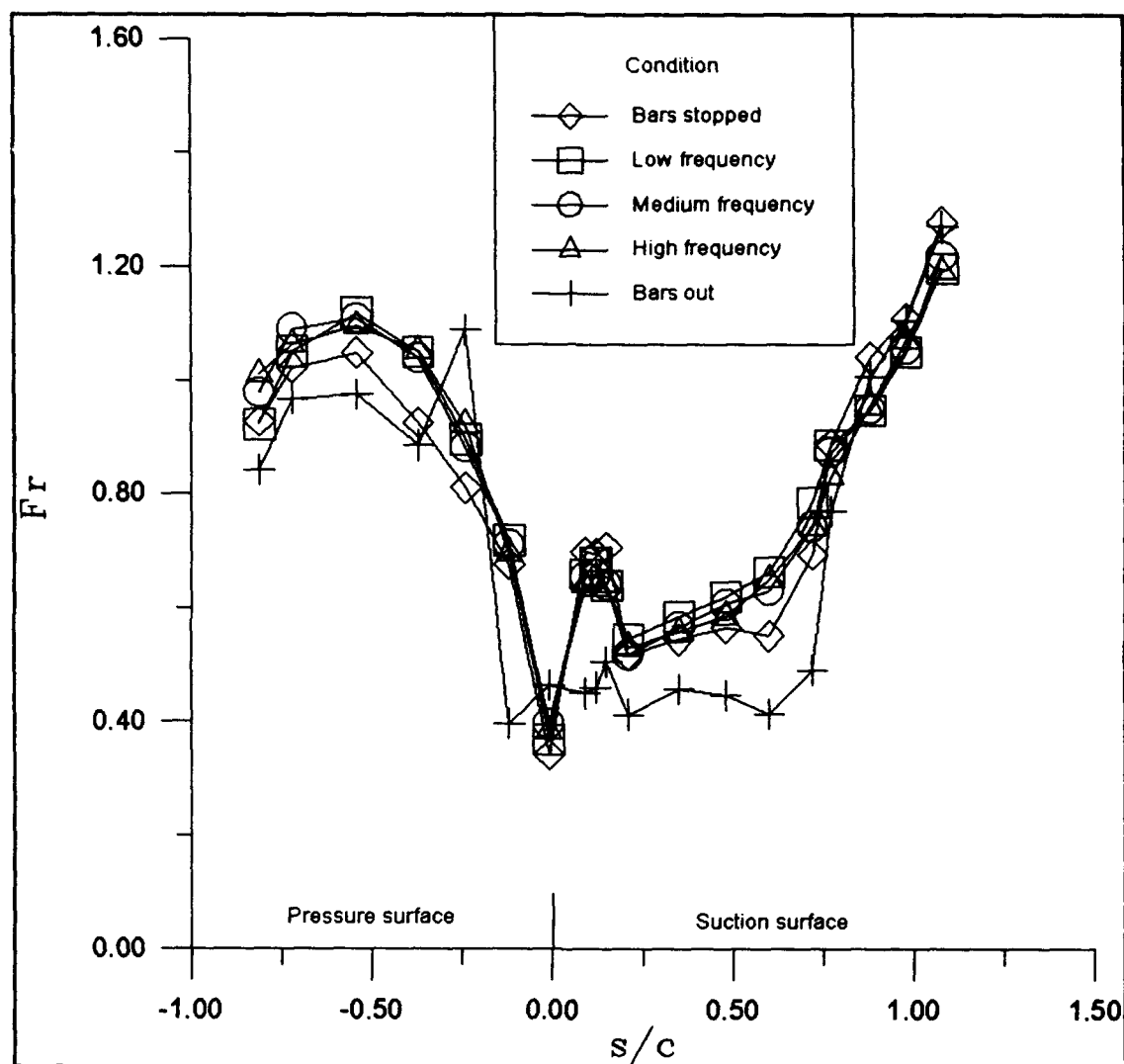
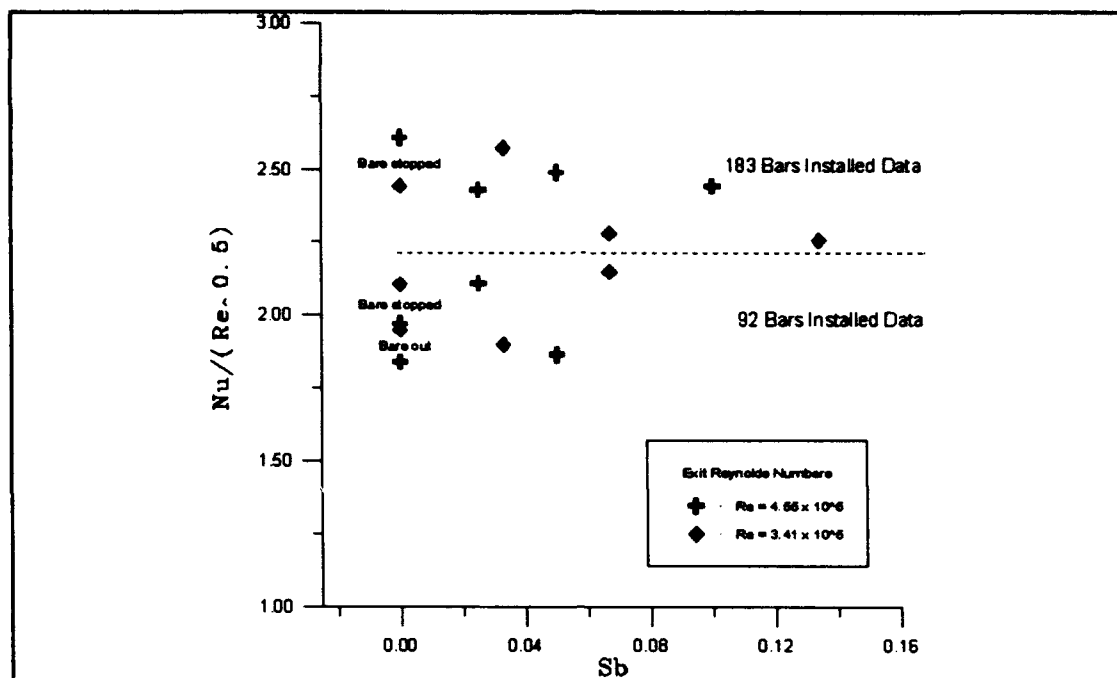
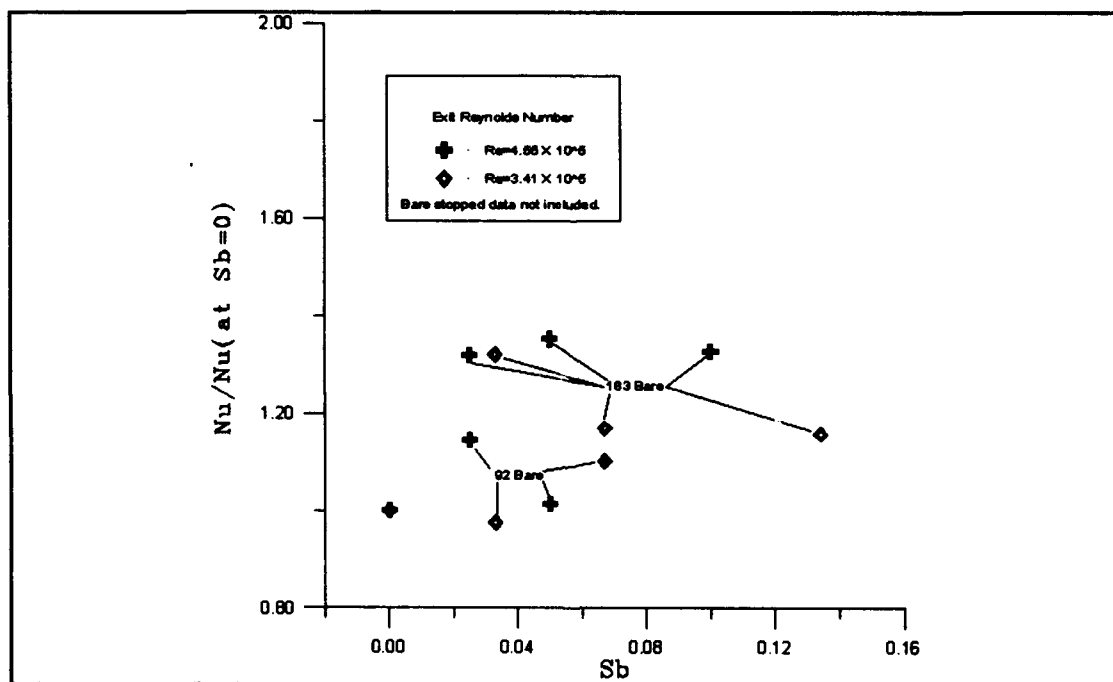


Figure 38 - Local Frössling number over the surface of the blade,  $Re_{exit} = 454,800$ .



**Figure 39** - Stagnation Frösslings number,  $Nu$  based on chord length,  $Re$  based on freestream velocity and chord length, versus bar passing Strouhal number.



**Figure 40** - Stagnation  $Nu_c$  over bar out  $Nu_c$  versus bar passing Strouhal number.

#### 4.4.3 Comparisons with Previous Work and Empirical Solutions

Comparison with Previous TCTF Work. Meschwitz (1991) used the TCTF to investigate the effect of imparting 10% freestream turbulence, using a turbulence grid, on the flow through the cascade. Figure 41 plots Meschwitz data at the medium  $Re_\infty$  condition (approximately 40 m/s) with the data obtained in this experiment.

As Figure 41 shows, the results of Meschwitz (1991) and this experiment are in very close agreement. There is virtually no difference between the turbulence driven heat transfer data of Meschwitz and the data from this experiment taken with the bars translating. This is contrary to the results of Doorly (1984), and Schultz, et al. (1986) who have shown that turbine blade heat transfer is affected differently by wakes than by freestream turbulence.

The answer to the contradiction lies in the time scales, mentioned in Chapter I and defined in Chapter II. The data of Doorly (1984) and Schultz, et al. (1986) was taken at engine representative conditions, including the wake passing time scales,  $S$ . For a representative turbine engine, with  $f_b \sim 12,000$ ,  $c \sim 25.4$  mm, and  $u_{ave} \sim 200$  m/s, the time scale is on the order of  $S_{engine} \sim 1.5$ . For this experiment, with  $f_b \sim 321$ ,  $c \sim 114.3$  mm, and  $u_{ave} \sim 45$  m/s, it is of order  $S_{cascade} = 0.82$ .

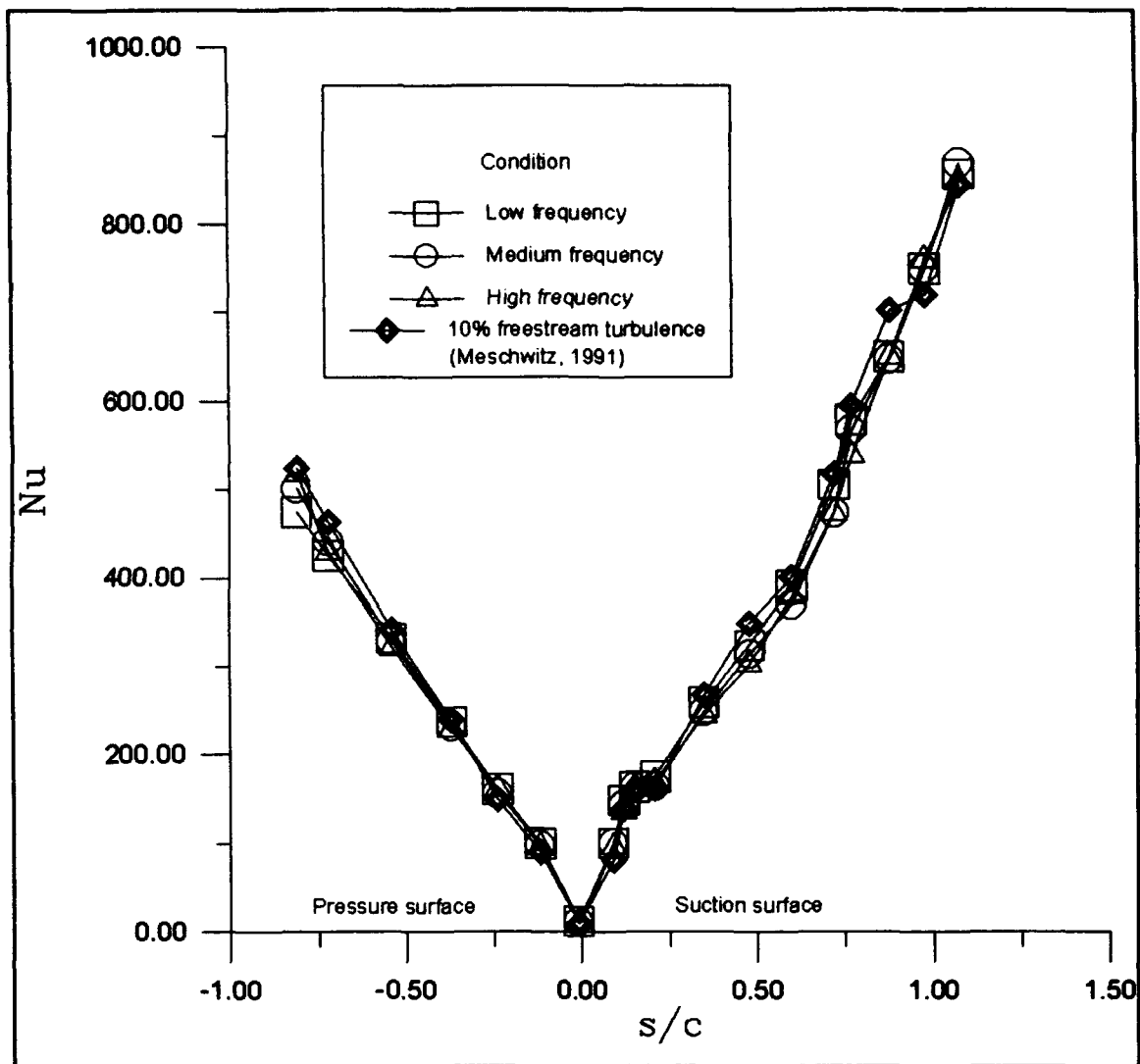


**Figure 41** - Nusselt numbers compared with Meschwitz's (1991) 10% turbulence data,  $Re_{exit} = 454,800$ .

It has also been noted that " . . . between wakes the level <of heat transfer at the stagnation point> corresponds to that of the undisturbed freestream (Doorly, 1984)."

Also, further along the blade there is a momentary transition of the boundary layer to turbulent, and thus an increase of heat transfer, associated with wake passage (Doorly, 1984). Liu, et al. (1989), in flat plate tests, discovered that the turbulent and laminar boundary layer patches convect down the boundary layer until, at some point on the blade, the boundary layer transitions to turbulent, where the effects of wake passage are no longer found.

The time resolved heat transfer and boundary layer results of Doorly (1984) and Liu, et al. (1989) suggest that the boundary layer has time to recover between wake passages. This allows the heat transfer of the blade to return to normal freestream conditions when a wake is not present. With the time scales involved in this experiment being much greater than those of Doorly (1984) and Schultz, et al. (1986), the boundary layer spends more time at the undisturbed state and thus the mean heat transfer will not reveal as much of the influence of the wake passages as those of engine representative condition experiments. But, more importantly, the bar speed with respect to the flow speed is small enough such that the wakes appear to be only freestream turbulence.



The results of the experiments run with only 92 bars installed (versus 183) support this argument as well. With only half of the bars installed, the coefficient of pressure and convective heat transfer coefficient curves were effected to a lesser degree than they had been with 183 bars installed, and there was still no bar passing frequency dependence. In effect, halving the number of bars only decreased the resulting turbulence from the wakes.

The results of one of the experiments of Dullenkopf, et al. (1990) tend to back up this claim. Using an apparatus similar to that of Doorly (1984), Dullenkopf found that for a very low inlet velocity the heat transfer results for low bar passing frequency were very close to the results for a run with a turbulence grid installed. This is what was seen in this experiment.

Comparison with Empirical Solutions. Figures 42-45 show the local  $Nu$  versus local  $Re$  for each surface of the blade and both freestream Reynolds numbers. Also plotted are laminar and turbulent empirical solutions developed by Eckert and Ambrok, respectively (Kays and Crawford, 1993), equations 17 and 18 in Chapter II. The empirical solution for the laminar case (eq. 17) was developed for an arbitrarily shaped body of constant temperature, and the turbulent relation is considered good for flow in nozzles and over rockets. However, these empirical relationships

fail to predict well the heat transfer of the cascade blade on the pressure surface.

On the suction surface the heat transfer progresses at slightly higher than laminar empirical solution values from  $Re_i = 50,000$  to  $250,000$  for  $Re_{exit} = 341,100$ , and  $Re_i = 100,000$  to  $300,000$  for  $Re_{exit} = 454,800$ , where it increases sharply to match the turbulent approximation. In these cases the boundary layer on the suction surface is most likely transitioning from laminar to turbulent.

On the pressure surface the predictions become worse. The measured heat transfer is much greater than the predicted until nearly the trailing edge. Dring, et al. (1986) and Doorly (1984) found that their values of  $h$  were also much greater than the predictions on the pressure surface and mention the possibility of Goertler vortex systems existing on the pressure surface. The existence of a vortex could significantly influence heat transfer and cause the rates to increase, as was seen in this experiment. However, without more experiments the presence of these Goertler vortices cannot be verified.

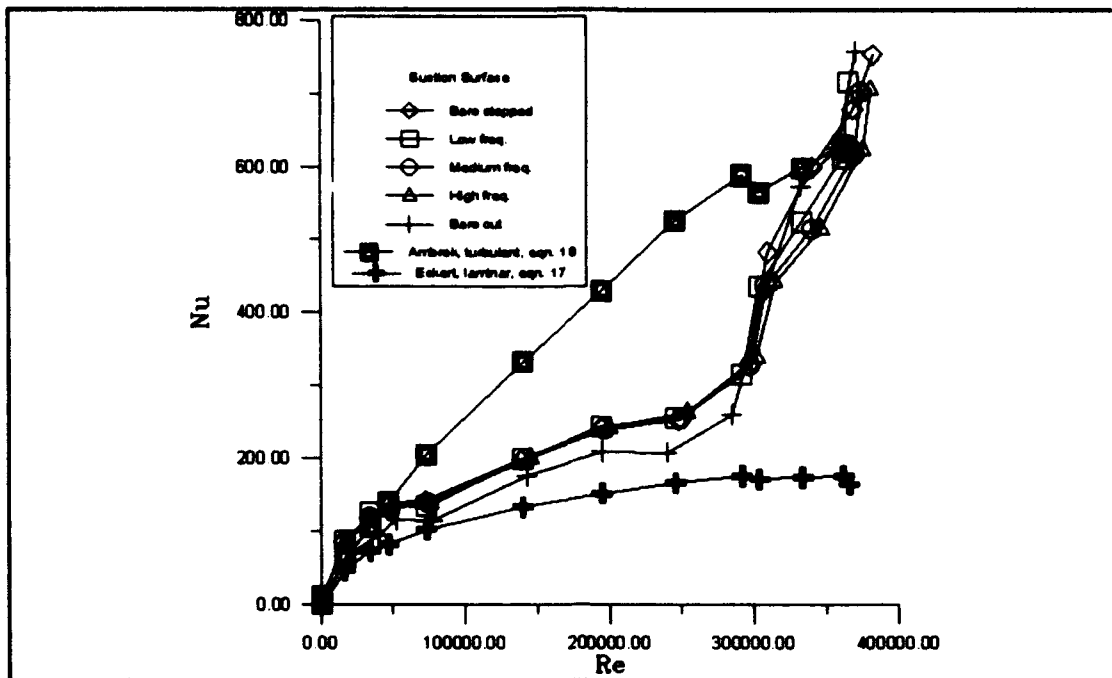


**Figure 42** - Comparison of analytical data and empirical solns. of  $Nu_i$  versus  $Re_i$ , suction surface,  $Re_{exit} = 341,100$ .

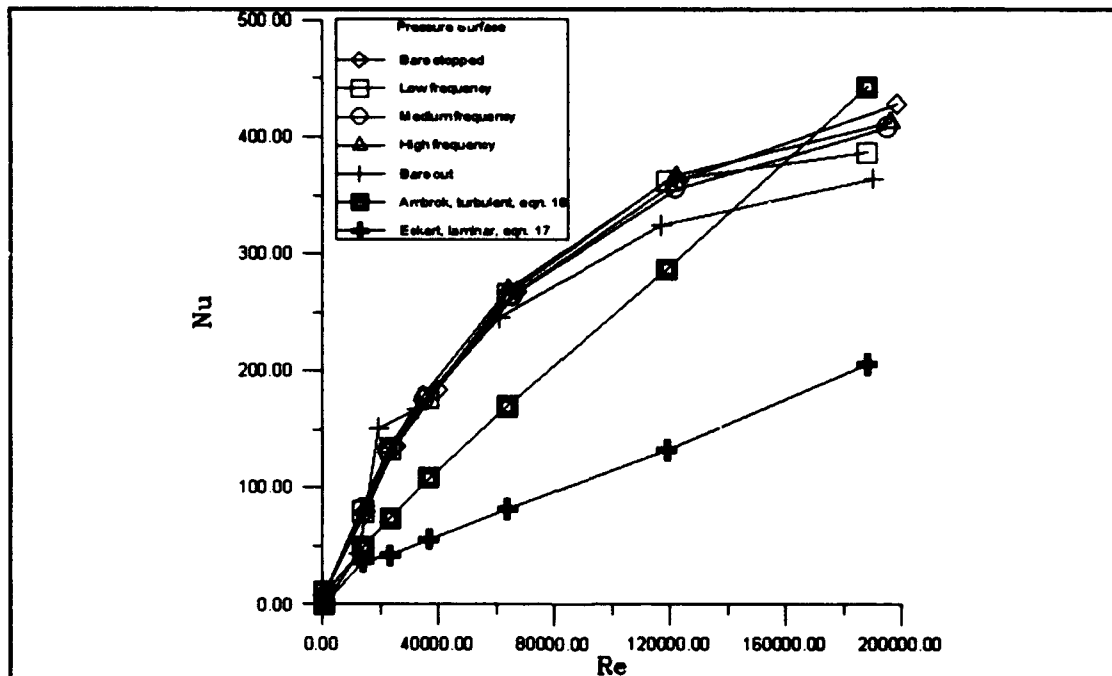


**Figure 43** - Comparison of analytical data and empirical solns. of  $Nu_i$  versus  $Re_i$ , pressure surface,  $Re_{exit} = 341,100$ .

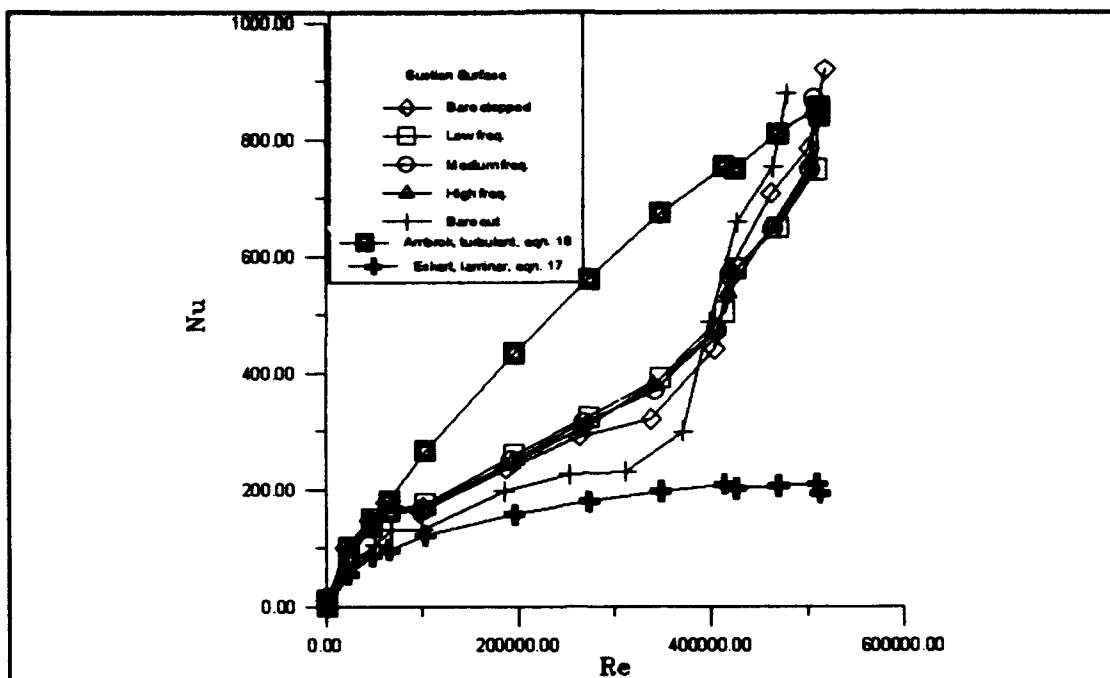


**Figure 44** - Comparison of analytical data and empirical solns. for  $Nu_i$  versus  $Re_i$ , suction surface,  $Re_{exit} = 454,800$ .

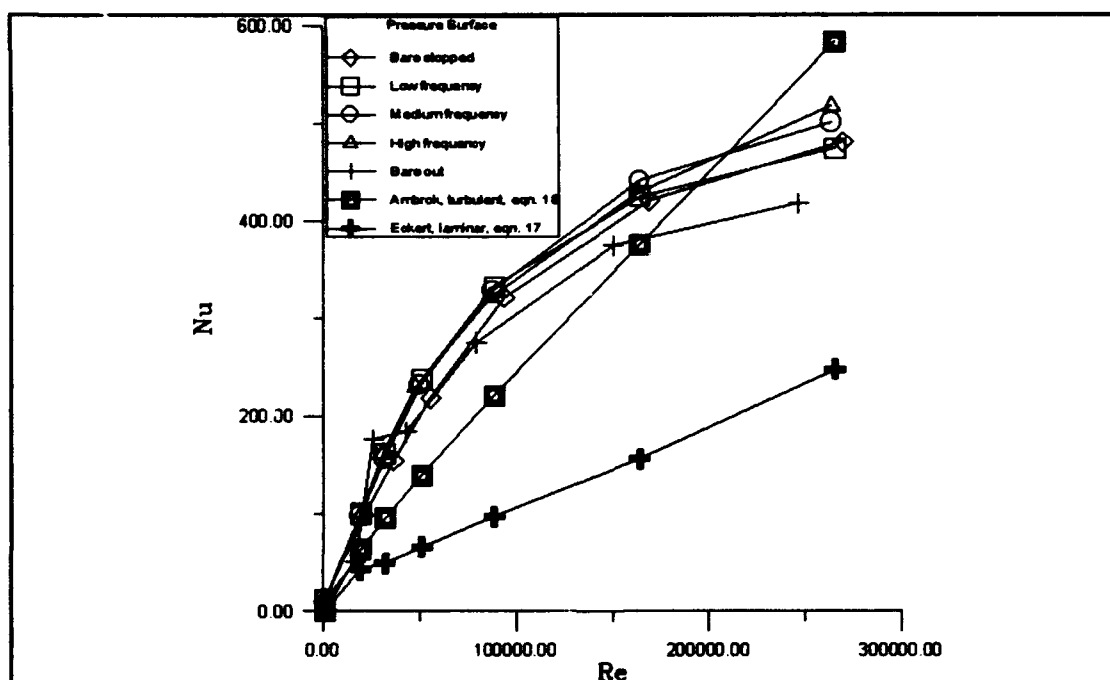


**Figure 45** - Comparison of analytical data and empirical solns. of  $Nu_i$  versus  $Re_i$ , pressure surface,  $Re_{exit} = 454,800$ .

## V CONCLUSIONS AND RECOMMENDATIONS

### 5.1 General

A study of the effects of wake passage on the mean heat transfer in a linear turbine cascade was undertaken. The parameters of interest were the freestream Reynolds number,  $Re_\infty$ , and bar passing frequency,  $f_b$ . Measurements of blade surface pressure and temperature of a heated foil resulted in calculations for convective heat transfer coefficient ( $h$ ), Nusselt number ( $Nu_t$  and  $Nu_c$ ), Stanton number ( $St$ ), and Frössling number ( $Nu/Re^{1/2}$ ). The results of the experiment and calculation of the above parameters were analyzed with and compared to the works of others, such as Doorly (1984), Dullenkopf, et al. (1990), Schultz, et al. (1986), and O'Brien (1988).

### 5.2 Apparatus

Many modifications were made to AFIT's TCTF to facilitate the translation of bars in the entrance to the cascade. Two different freestream Reynolds numbers and five bar conditions (out, installed and stationary, installed and translating at three different speeds) were investigated. A computer controlled data acquisition unit was employed to gather the pressure and temperature data. Flow angles and bar passing frequencies were input by hand to the computer. The computer then ran the data reduction software to

calculate the required heat transfer parameters.

### 5.3 Wake Effects

This experiment found that the passing of wakes had a great deal of effect on the heat transfer in the turbine cascade. However, the primary change in mean heat transfer was due to the installation of the bars in the tunnel, translating or not. The presence of the bars affected the mean heat transfer of the blade in the same manner as did the installation of a turbulence grid upstream of the cascade generating nearly 10% freestream turbulence (Meschwitz, 1991). This result is contrary to the results of other researchers, specifically Doorly (1984) who suggests that the effects of wake passing and freestream turbulence are different.

The reason for this apparent contradiction lies in the examination of the time scales employed in the experiments. Whereas Doorly had a time scale representative of a turbine engine,  $S_{engine} = 1.5$ , this experiment could not achieve a time scale greater than  $S_{cascade} = 0.82$ . The lengthened time between wake passings in this experiment resulted in the lessening of the effect of the higher, wake induced, transient heat transfer on the mean heat transfer of the blade.

Some changes in the geometric stagnation point (point

2) heat transfer were caused by changing the frequency of bar passing. Other studies, Doorly (1984) and O'Brien (1988), have determined this to be a natural result of the passing of wakes across a surface.

Comparisons to 2-D empirical calculations for heat transfer proved to be interesting. On the suction surface the predictions held very well. They indicate that flow is laminar over the first half of the blade's surface then transitions to fully turbulent flow at the trailing edge. Over the pressure surface the predictions proved to be poor. The measured heat transfer over nearly the entire pressure surface is a great deal higher than the turbulent prediction. It is possible that this is the result of Goertler vortices developing on the blade creating a three-dimensional effect that is not modeled by the 2-D predictions.

#### 5.4 Future Experiments

The interest in this area tends to be concerned with the transient or time resolved effects of wake passing on heat transfer. In the future it might be possible to instrument the TCTF with surface mounted gages that are capable of measuring the fluctuations of heat transfer with respect to wake passage in real time. Combined with a pressure transducer that is capable of real time pressure

measurement and X-wire anemometry to determine the velocity and transient turbulence scales, the TCTF could be a tremendous asset in learning the transient effects of the passage of a wake on heat transfer.

If these are not possible, the manufacture of a more densely instrumented blade is important. With only 23 static pressure ports and blade foil thermocouples, it is very difficult to track the location of the stagnation point. Even if no more channels are added, a new blade should pack the points at the leading edge and station them less densely at the remainder of the blade, as the characteristics are better understood further down the blade's surface.

Also, if a new blade is being made, a new heat transfer foil should be made. The present heat transfer foil has a problem with hot spots at the power input bus bars due to current density (Meschwitz, 1991). It is for this reason that the heat transfer data taken from points 9, 10 and 12 had to be discarded.

Finally, from a practical standpoint there needs to be a few changes made to the TCTF setup. First, the Scanivalve pressure transducer should be foregone in favor of a high speed computer controlled pressure transducer system. Accuracy will improve, but more important, the speed of pressure data acquisition will take an order of magnitude



leap. Secondly, improvements should be made to the bar translating system. A few simple improvements to improve the stability of the belt and bars would increase the bar passing frequency to a great degree. Such improvements could include modifying the bars to include a bulbous end to prevent it from sliding out of the drive belt during operation. Also, the free ends of the bars could be attached loosely so that they follow one another and remain evenly spaced.

Last, a cover should be made to enclose the slots cut in the plexiglass top that the bars pass through. The "home made" seal that was used for this experiment was difficult to install.

### List of References

- Acree, J.L. Turbulence Scales in the Passage of a Linear Turbine Cascade. MS Thesis, AFIT/GAE/ENY/90D-01. School of Engineering, Air Force Institute of Technology (AU), Wright-Patterson AFB OH, December 1990.
- Ainsworth, R.W., and J.E. LaGraff. Wake Interaction Effects on the Transition Process on Turbine Blades. AFOSR-TR-89-1342, 1989.
- Braunschneider, J. Analysis of the effect of Wake Passing on Losses in a Linear Turbine Cascade. MS Thesis, AFIT/GAE/ENY/93D-6. Graduate School of Engineering, Air Force Institute of Technology (AU), Wright-Patterson AFB OH, December 1993.
- Dixon, S.L. Fluid Mechanics, Thermodynamics of Turbomachinery. New York: Pergamon Press, 1989.
- Doorly, D.J. Study of the Effect of Wake-Passing on Turbine Blades. PhD dissertation. Oxford University, England, 1984. (PB84-234970)
- Doorly, D.J., and M.L.G. Oldfield. "Simulation of the Effects of Shock Wave Passing on a Turbine Rotor Blade," Transactions of the ASME, 107. 998-1006 (October 1985).
- Dring, R.P., M.F. Blair, H.D. Joslyn, G.D. Power, and J.M. Verdon. Effects of Inlet Turbulence and Rotor/Stator Interactions on the Aerodynamics and Heat Transfer of a Large-Scale Rotating Turbine Model. Contract NAS3-23717. NASA Contractor Report 4079.
- Dullenkopf, K., A. Schultz, and S. Wittig. "Effect of Incident Wake Conditions on the Mean Heat Transfer of an Airfoil," Gas Turbine and Aeroengine Congress and Exposition. Brussels, June 1990. (90-GT-121)
- Dunn, M.G., and R.E. Chupp. "Time-Averaged Heat-Flux Distributions and Comparison with Prediction for the Teledyne 702 HP Turbine Stage," Gas Turbine Conference and Exhibition. New York: ASME, 1987. (87-GT-120)

- Galassi, L. Turbulence Scale Effects on Heat Transfer in a Linear Turbine Cascade. MS Thesis, AFIT/GAE/ENY/89D-10. School of Engineering, Air Force Institute of Technology (AU), Wright-Patterson AFB OH, December 1989.
- Hilditch, M.A., and R.W. Ainsworth. "Unsteady Heat Transfer Measurements on a Rotating Gas Turbine Blade," Gas Turbine and Aeroengine Congress and Exposition. Brussels, June 1990. (90-GT-175)
- Johnson, A.B., M.J. Rigby, M.L.G. Oldfield, R.W. Ainsworth, and M.J. Oliver. "Surface heat Transfer Fluctuations on a Turbine Rotor Blade Due to Upstream Shock Wave Passing," Journal of Turbomachinery, 111: 105-115 (April 1989).
- Kays, W.M. and M.E. Crawford. Convective Heat and Mass Transfer. New York: McGraw-Hill, Inc. 1993.
- Liu, X., and W. Rodi. "Measurement of Unsteady Flow Over and Heat Transfer From a Flat Plate," Gas Turbine and Aeroengine Congress and Exposition. Toronto, June 1989. (89-GT-2)
- Meschwitz, S.G. The Effect of Angle of Incidence and Reynolds Number on Heat Transfer in a Linear Turbine Cascade. MS Thesis, AFIT/GAE/ENY/91D-06. School of Engineering, Air Force Institute of Technology (AU), Wright-Patterson AFB OH, December 1991.
- Modest, Michael F. Radiative Heat Transfer. New York: McGraw-Hill, Inc. 1993.
- Oates, Gordon C., editor. Aerothermodynamics of Aircraft Engine Components. New York: American Institute of Aeronautics and Astronautics, 1985.
- O'Brien, J.E. "Effects of Wake Passing on Stagnation Region Heat Transfer," Winter Annual Meeting of the American Society of Mechanical Engineers. 17-28. New York: ASME, 1988.
- Rigby, M.J., A.B. Johnson, M.L. Oldfield and T.V. Jones. "Temperature Scaling of Turbine Blade Heat Transfer with and without Shock Wave Passing," 9th International Symposium on Air Breathing Engines. Athens, Sept. 1989.

Schultz, D.L., and J.E. LaGraff. Wake Interaction on the Transition Process on Turbine Blades. AFOSR-TR-87-0108, 1986.

Tran, Le T., and Dale B. Taulbee. "Prediction of Unsteady Rotor-Surface Pressure and Heat Transfer from Wake Passings," International Gas Turbine and Aeroengine Congress and Exposition. Orlando, June 1991. (91-GT-267)

# APPENDIX I

The temperatures are very sensitive to the ambient room temperature. For the 92 bars installed cases the test facility was heated to approximately 82 degrees F. The other runs were done at approximately 60 - 65 degrees F. Thus the differences between the temperature data for the various conditions.

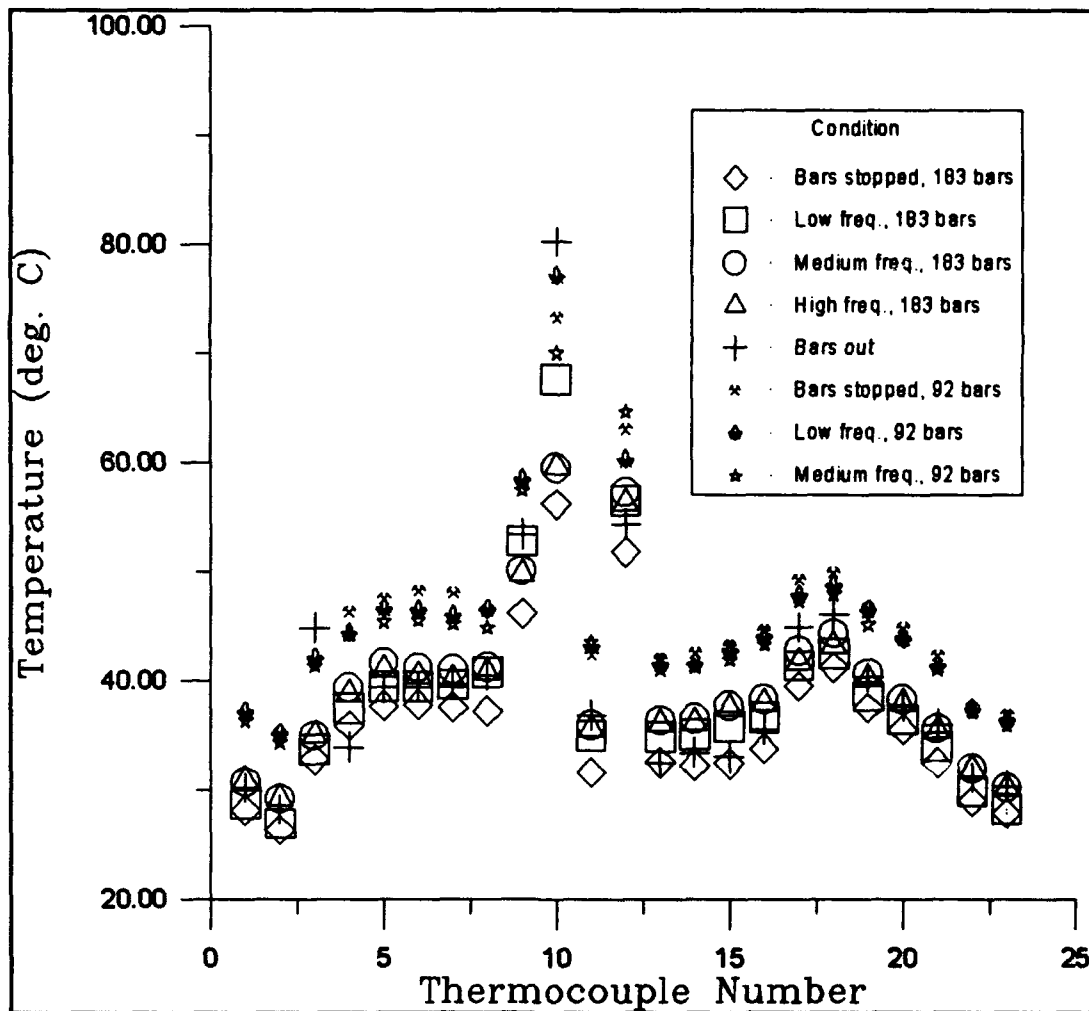


Figure 46 - Raw temperature data for the 23 exterior thermocouples,  $Re_{exit} = 341,100$ .

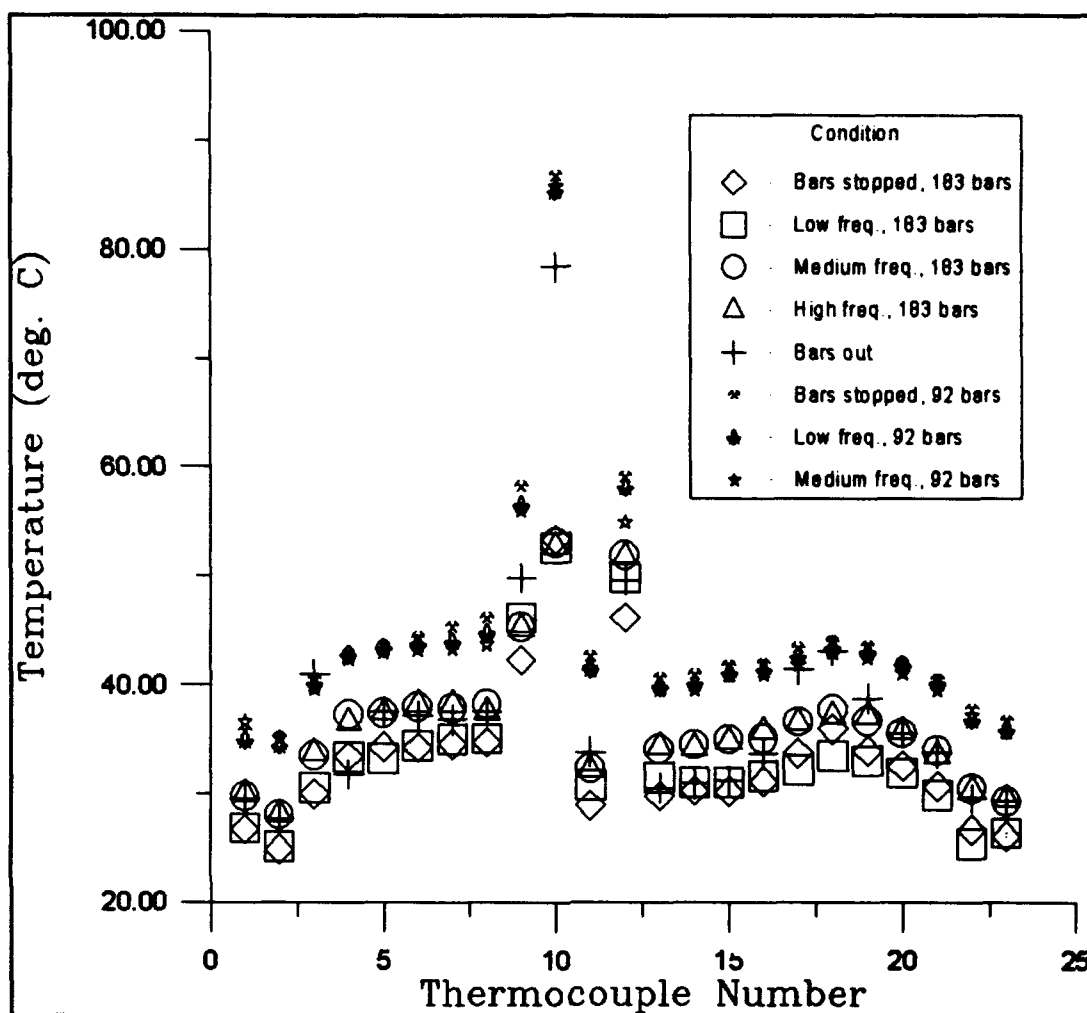


Figure 47 - Raw temperature data for the 23 exterior thermocouples,  $Re_{exit} = 454,800$ .

## VITA

Captain Scott Allen was born in Landstuhl, Germany and Graduated from Layton High School, Utah, in 1984. He attended the United States Air Force Academy and graduated in 1988 with a Bachelor of Science degree in Aeronautical Engineering and received a regular commission into the United States Air Force. His first assignment was to the Tactical/Fighter/Trainer System Program Management Division at Kelly AFB, TX as a structural engineer, from 1988 until entering the AFIT Graduate School of Engineering in 1992.

### Permanent Address:

Rt. 2 Box 96

New Martinsville, WV 26155

# REPORT DOCUMENTATION PAGE

Form Approved  
OMB No 0704-0188

Public reporting burden for this collection of information is estimated to average 1 hour per response, including the time for reviewing instructions, searching existing data sources, gathering and maintaining the data needed, and completing and reviewing the collection of information. Send comments regarding this burden estimate or any other aspect of this collection of information, including suggestions for reducing this burden, to Washington Headquarters Services, Directorate for Information Operations and Reports, 1215 Jefferson Davis Highway, Suite 1204, Arlington, VA 22202-4302, and to the Office of Management and Budget, Paperwork Reduction Project (0704-0188), Washington, DC 20503.

1. AGENCY USE ONLY (Leave blank)

2. REPORT DATE  
DEC 93

3. REPORT TYPE AND DATES COVERED  
Master's Thesis

4. TITLE AND SUBTITLE

ANALYSIS OF THE EFFECTS OF WAKE PASSAGE ON HEAT  
TRANSFER IN A LINEAR TURBINE CASCADE

5. FUNDING NUMBERS

6. AUTHOR(S)

Capt Kevin Scott Allen

7. PERFORMING ORGANIZATION NAME(S) AND ADDRESS(ES)

Air Force Institute of Technology,  
WPAFB OH 45433-6538

8. PERFORMING ORGANIZATION  
REPORT NUMBER

AFIT/GAE/ENY/93D-2

9. SPONSORING/MONITORING AGENCY NAME(S) AND ADDRESS(ES)

Dr Dick Rivir  
WL/POTC WPAFB OH 45433-6583  
Wright-Patterson AFB OH 45433

10. SPONSORING/MONITORING  
AGENCY REPORT NUMBER

11. SUPPLEMENTARY NOTES

12a. DISTRIBUTION/AVAILABILITY STATEMENT

Approved for public release; distribution unlimited

12b. DISTRIBUTION CODE

13. ABSTRACT (Maximum 200 words)

This study investigated the effect of wake passage on the heat transfer in a linear turbine cascade. The apparatus used was the Air Force Institute of Technology linear Turbine Cascade Test Facility (TCTF). The TCTF was fitted with a belt and pulley system to facilitate a series of translating bars. The bars, when passed upstream of the cascade, created a series of wakes. The parameters varied were freestream model Reynolds number and bar conditions, i.e., bars in, bars out, and bar passing frequency. One blade in the TCTF was instrumented to allow pressure and temperature measurements at discrete points on the blade's surface. From the pressure and temperature data the convective heat transfer coefficient at these discrete locations was calculated. Results were compared to previous TCTF heat transfer data, empirical solutions, and other wake passage experiments. For all tests with closely spaced bars, the effect of wake passing on the heat transfer of the blade was similar to the effect of grid-generated 10% freestream turbulence on the cascade.

14. SUBJECT TERMS

Heat Transfer; Heat Flux; Turbine Cascade; Turbulence; Turbine  
blades; Wake; Interactions; Rods; Instrumentation; Transitions

15. NUMBER OF PAGES

93

16. PRICE CODE

17. SECURITY CLASSIFICATION  
OF REPORT

Unclassified

18. SECURITY CLASSIFICATION  
OF THIS PAGE

Unclassified

19. SECURITY CLASSIFICATION  
OF ABSTRACT

Unclassified

20. LIMITATION OF ABSTRACT

UL